PROTEINS
STRUCTURE ■ FUNCTION ■ BIOINFORMATICS

Computational prediction and analysis of the DR6–NAPP interaction

Sergei Y. Ponomarev[1] and Joseph Audie[1,2]*

[1] CMD Bioscience, LLC, 554 Boston Post Rd #318, Orange, Connecticut 06477

[2] Department of Chemistry, Sacred Heart University, 5151 Park Ave, Fairfield, Connecticut 06825

ABSTRACT

Alzheimer's disease (AD) is a progressive neurodegenerative disorder that involves a devastating clinical course and that lacks an effective treatment. A biochemical model for neuronal development, recently proposed by Nikolaev et al., that may also have implications for AD, hinges on a novel protein–protein interaction between the death cell receptor 6 (DR6) ectodomain and an N-terminal fragment of amyloid precursor protein (NAPP), specifically, the growth factor-like domain of NAPP (GFD NAPP). Given all of this, we used a pure computational work-flow to dock a binding competent homology model of the DR6 ectodomain to a binding competent crystal structure of GFD NAPP. The DR6 homology model was built according to a template supplied by the neurotrophin p75 receptor. The best docked model was selected according to an empirical estimate of the binding affinity and represents a high quality model of probable structural accuracy, especially with respect to the residue-level contribution of GFD NAPP. The final model was tested and verified against a variety of biophysical and theoretical data sets. Particularly, worth noting is the excellent observed agreement between the theoretically calculated DR6–GFD NAPP binding free energy and the experimental quantity. The model is used to provide a satisfying structural and energetic interpretation of DR6–GFD NAPP binding and to suggest the possibility of and a mechanism for spontaneous apoptosis. The evidence suggests that the DR6–NAPP model proposed here is of probable accuracy and that it will prove useful in future studies, modeling work, and structure-based AD drug design.

Proteins 2011; 79:1376–1395.

Key words: Alzheimer's disease; death cell receptor 6; N-terminal amyloid precursor protein; homology modeling; implicit solvent; structure refinement; energy minimization; rigid-body protein–protein docking; binding free energy; scoring and ranking.

INTRODUCTION

Recently, Nikolaev et al. described a novel molecular mechanism to account for axonal pruning and neuronal cell death during physiological development.[1] They further hypothesized that the new mechanism might have implications for the pathophysiology of Alzheimer's disease (AD). According to their proposed developmental model, tropic factor deprivation results in amyloid precursor protein (APP) proteolysis, culminating in the release of an N-terminal APP fragment (NAPP) into the extracellular milieu. NAPP then serves as a ligand for death cell receptor 6 (DR6), a novel member of the tumor necrosis factor receptor (TNFR21) family. Binding to the DR6 ectodomain results in the subsequent downstream activation of caspase-3 and caspase-6, respectively, resulting in accelerated neuronal apoptosis, neuronal degeneration, axonal degeneration, and the physiological sculpting of nerve connections in the developing brain. Importantly, Nikolaev et al. performed an experiment using an antibody specific for the growth factor-like domain (GFD) of NAPP [anti-GFD NAPP (22C11)] that blocked DR6 binding, suggesting a key role for GFD-mediated binding to DR6.

Nikolaev et al. hypothesized that this physiological pathway could be hijacked in the adult brain, possibly resulting in AD. The DR6–GFD NAPP protein–protein interaction, then, is a key event in the pathway described by Nikolaev *et al.* and possibly in the progression of AD.

Clearly, an atomic-level structure of the DR6–GFD NAPP interaction would be of considerable interest. Such a structure could be used to guide the rational design of molecular antagonists of the DR6–GFD NAPP interaction. Our collective theoretical understanding of the interaction and our ability to design and interpret experiments would also benefit from a structural model. Unfortunately, such a molecular model is lacking.

Over the near term, progress can be made toward the development of a high-quality DR6–GFD NAPP structural model

Additional Supporting Information may be found in the online version of this article.

Sergei Y. Ponomarev and Joseph Audie contributed equally to this work.

Conflict of interest: J.A. is a cofounder of CMDBioscience.

*Correspondence to: Joseph Audie, Department of Chemistry, Sacred Heart University, 5151 Park Ave, Fairfield, Connecticut 06825.
E-mail: audiej@sacredheart.edu.

Received 21 June 2010; Revised 2 November 2010; Accepted 24 November 2010
Published online 13 December 2010 in Wiley Online Library (wileyonlinelibrary.com).
DOI: 10.1002/prot.22962

through the application of computational methods, specifically, homology modeling and protein–protein docking methods. Indeed, numerous studies have been published that describe the successful use of multimethod computational work-flows to model protein–protein interactions.[2–10] Where possible, such studies use protein crystal structures. However, studies have also been published that relied on the use of protein homology models. Either way, the studies typically proceed by using the protein structures as inputs to protein–protein docking algorithms. In a third step, the model complexes predicted by the docking algorithm are subject to a refinement or optimization step. Very often, the optimized model complexes are then scored and ranked according to some quantitative criterion. Finally, the best ranked models are tested against the available experimental data, typically mutational data, and inferences are drawn accordingly. Importantly, the critical assessment of prediction of interactions or the community-wide CAPRI experiment includes the use of homology models and multimethod, docking, refinement, and scoring approaches.[11,12] It is also worth noting that recent work has focused on systematically studying protein–protein docking with the use of homology models, with encouraging results.[13] A fair interpretation of the literature suggests that in the case of rigid-body docking with binding competent receptor and ligand conformations, protein–protein docking algorithms and refinement strategies can be used to suggest structurally acceptable protein–protein structural models with a >50% success rate.[14]

Perhaps the key obstacle to successful structure prediction is the scoring problem or the problem of accurately scoring and ranking the docked complexes.[15,16] The ideal scoring function would be physics-based, would accurately predict native and non-native binding affinities, and would be computationally inexpensive. Importantly, a recently described empirical free energy function seems to satisfy these conditions.[17–19] Thus, a viable scoring function is now available to help guide final model selection and analysis.

Given all of this, we labored to produce a theoretical model of the DR6–GFD NAPP interaction through the use of a multimethod computational work-flow. A search of the Protein Data Bank (PDB; www.pdb.org) resulted in the identification of a binding competent monomeric crystal structure of the GFD NAPP.[20,21] Unfortunately, a structure of the DR6 ectodomain is unavailable. Luckily, a binding competent crystal structure of the neurotrophin p75 receptor ectodomain in 2:1 complex with nerve growth factor (NGF) is available.[22] The p75 ectodomain shares good sequence identity with the DR6 sequence. Like DR6, p75 is a transmembrane protein, is a member of the TNFR family (TNFR16), appears to play a role in apoptosis and in AD, and is known to bind NAPP.[1,23] Thus, like the DR6 ectodomain, the p75 ectodomain is stabilized by numerous disulfide bonds and is organized into several cysteine-rich domains (CRDs) that probably play a role in binding.[24] The p75–NGF interaction has also been the subject of previous modeling and docking studies.[4,7] Thus, using p75 as a template structure, we were able to construct a high quality and binding competent homology model of the DR6 ectodomain. The binding competent GFD NAPP and DR6 structures were then submitted to a rigid-body docking program. The docked complexes were optimized through rigid-body energy minimization. Final scoring and ranking was handled using the above-described empirical free energy function. Importantly, much of the modeling work-flow was previously validated on the p75–NGF interaction (see Supporting Information). The entire computational procedure ultimately converged on a single, structurally and energetically realistic DR6–GFD NAPP model of probable accuracy.

The a priori results of the pure computational work-flow suggested that we had succeeded in constructing a roughly accurate model of the DR6–GFD NAPP interaction and that additional a posteriori testing was warranted. Thus, the final model was verified against the available biophysical data and a novel theoretical dataset that was generated using an independent computational procedure for predicting protein–protein interface residues. Perhaps most importantly, the theoretical binding affinity implied by our DR6–GFD NAPP model is shown to be in quantitative agreement with the experimental value reported by Nikolaev et al. To the best of our knowledge, such absolute and quantitative comparative free energy testing represents a milestone in theoretical protein–protein model construction and testing. Encouraged by our modeling results, we decided to consider some of the biophysical and biological interpretations and implications that are suggested by the model. In particular, the model suggests a plausible physical basis for DR6–GFD NAPP recognition and suggests the possibility of and a mechanism for spontaneous or ligand-free cellular apoptosis.

In summary, we are confident that the rigid-body binding geometry of our model is roughly accurate and that many of the interface residues predicted by our model are the interface residues that will one day be revealed by experiment, especially with regards to the GFD NAPP contribution. Thus, the available data suggests that our DR6–GFD NAPP structural interaction model is of probable accuracy and that it should prove useful in structure-based AD drug design and in the design, analysis, and interpretation of experiments.

METHODS

Recently, Nikolaev et al. described a protein–protein interaction between DR6, a transmembrane protein, and the N-terminal domain (1–286) of APP (NAPP). The DR6–NAPP interaction is of considerable interest as it might play a role in AD pathogenesis. Biophysical evidence suggests that the DR6–NAPP interaction specifically involves the DR6 ectodomain (67–211) and the GFD

of NAPP (28–123). We propose to build and validate a DR6–GFD NAPP model using a multimethod computational work-flow and by testing it against biophysical and theoretical datasets.

Building the DR6–GFD NAPP interaction model: computational details

Briefly, our modeling work-flow combined crystal structure evaluation (GFD NAPP), homology modeling (DR6), and homology model refinement through energy minimization. In an effort to ensure model quality, extensive quality tests were performed along the way. The goal here was to validate the GFD NAPP and DR6 structures as representing high quality and binding competent conformations, suitable for subsequent rigid-body docking. Ultimately, we relied on rigid-body protein–protein docking, rigid-body energy minimization, and molecular mechanics-based and empirical-based free energy scoring to suggest a single, viable DR6–GFD NAPP interaction model for further testing and analysis.

Modeling and evaluating the structure of GFD NAPP

Rossjohn *et al.* have solved the crystal structure of residues 28–123 of GFD NAPP at 1.8 Å resolution.[20] The structure is available in the PDB (http://www.pdb.org/pdb/home/home.do) with PDB identifier 1mwp. The high quality of the GFD NAPP crystal structure was verified using standard tools. Comparison with a second, lower resolution but bound NAPP dimer structure (PDB code: 3ktm) suggests that the 1mwp GFD NAPP structure represents a realistic binding competent conformation.[25] As such, we used the 1mwp structure in this study and docked it to a homology model of the DR6 ectodomain.[15] All protein models and pictures, with an exception of Figure 8(B), which was done in VMD, were prepared using Swiss PDB Viewer (http://spdbv.vital-it.ch/).[26,27]

Modeling the structure of the ectodomain of DR6

We used the I-TASSER homology modeling server (http://zhanglab.ccmb.med.umich.edu/I-TASSER/) to construct a binding competent theoretical model of the DR6 ectodomain.[28–31] Toward that end, we submitted DR6 residues 67–211 to the I-TASSER server. The I-TASSER server builds homology models through an exhaustive process that involves automatic template selection, fragment reassembly of aligned regions, ab initio modeling of unaligned regions, clustering, energy evaluation, and the optimization of a model's hydrogen bonding network. Ultimately, we selected the top-ranked I-TASSER DR6 model, based on the template supplied by the bound crystal coordinates of the neurotrophin receptor p75 in complex with the neurotrophin (NGF) ligand (PDB code: 1sg1, chain X), for further analysis and eventual docking.[22]

Evaluating the quality of the I-TASSER DR6 ectodomain homology model

Homology model construction is typically followed by visual and quantitative model evaluation. Importantly, the I-TASSER server automatically calculates and outputs various quality scores to assist end-users in model evaluation and selection. In particular, I-TASSER calculates an overall target quality score and a predicted target TM score and RMSD score. The quality of our DR6 ectodomain homology model was further assessed according to a Ramachandran map analysis and through the use of three independent server-based methods: ProSA, Qmean, and DFIRE.[27,32–35] The ProSA server is available at: https://prosa.services.came.sbg.ac.at/prosa.php. Qmean and DFIRE were accessed through the SWISS-MODEL server (http://swissmodel.expasy.org/). All three servers use disparate methods to calculate quantitative scores that can be used to asses model quality and guide model selection.

Refining the structure of the I-TASSER ectodomain DR6 model

We used energy minimization, along with the Amber99 force field and the GB/SA implicit solvent model, to refine our DR6 ectodomain model. A termination criterion of 0.5 kcal/mol was applied, and convergence was achieved. All calculations were carried out using the TINKER molecular modeling package (http://dasher.wustl.edu/tinker/).[36] The energy-minimized I-TASSER DR6 ectodomain homology model was then used in the rigid-body protein–protein docking study.

Using rigid-body docking to model the interaction between the ectodomain of DR6 and GFD NAPP

Our primary goal was to generate a reasonably accurate model of the interaction between the DR6 ectodomain and GFD NAPP. To achieve this goal, we used the refined I-TASSER DR6 ectodomain model along with the GFD NAPP crystal structure as inputs to the ClusPro Docking server, version 1.0 (http://nrc.bu.edu/cluster/cluspro_v1.cgi).[37,38] By default, the ClusPro server docks receptor (DR6) and ligand (GFD NAPP) structures using version 1.0 of the DOT rigid-body docking algorithm (http://www.sdsc.edu/CCMS/DOT/). The top 20,000 complexes generated by DOT are then filtered according to electrostatic and desolvation energies, and the top 2,000 complexes are retained for further processing. The retained 2,000 conformations are then clustered according to interface RMSD and the top 10 docked models, following a short Charrm19 energy minimization, are made available for download. The top 10 ClusPro models probably capture most of the important rigid-body binding geometries and provide excellent starting structures for further refinement and analysis. The ClusPro docking methodology was validated using the 1sg1 crystal structure (see Supporting Information).

Refining, scoring, and ranking the docked DR6–GFD models

Ultimately, we sought to narrow the top 10 ClusPro models down to a single physically realistic docked configuration. To accomplish this, the binding affinities of the top 10 ClusPro conformations were estimated in a hierarchical fashion. First, all 10 complexes were relaxed and optimized through rigid-body energy minimization using the Charmm19 force field. Next, a pseudo-binding affinity ($\Delta G_{\text{bind,MM-GB/SA}}$) was calculated for all 10 models using the Charmm19 molecular-mechanics force field and GB/SA implicit solvent model (MM-GB/SA). All calculations were made using TINKER and default settings. Finally, ClusPro-generated complexes with negative pseudo-binding affinities ($\Delta G_{\text{MM-GB/SA}} < 0$) were scored using a recently described empirical free energy function that is available through CMDBioscience (http://www.cmdbioscience.com/).[17–19]

The CMDBioscience approach to protein–protein and protein–peptide binding free energy prediction ($\Delta G_{\text{bind,empirical}}$) involves the use of a novel, fast, physics-based, empirical free energy function. The function is a six-term, regression-weighted expression and is given by,

$$\Delta G_{\text{bind,empirical}} = -0.79\Delta X_{+/-} + 0.075\Delta X_{\text{c/s}} - 0.65X_{\text{sb}} - 0.86X_{\text{hb}} - 0.00089X_{\text{gap}} - 0.089\Delta X_{\text{tor}} - 0.33 \quad (1)$$

The first two terms refer to binding induced changes in the total number of solvent-exposed charged (N-terminal nitrogen atoms, Arg and Lys side chain nitrogen atoms; O-terminal oxygen atoms, Asp and Glu side-chain carboxyl oxygen atoms; by default, His is treated as uncharged) and hydrophobic atoms (C and S atoms), respectively. The third and fourth terms refer to the total number of hydrogen bonds and the net number (difference between favorable and unfavorable charge–charge contacts) of short-range ($\leq$4 Å) charge–charge or salt bridge interactions across the protein–protein interface. The contributions of these pairwise interface hydrogen bonding and salt bridge interactions are penalized according to the degree of solvent exposure, such that if the average solvent exposure is greater than some experimentally derived threshold value, energetic penalties are added to Eq. (1). The final three descriptors, in order, refer to the interface gap or void volume, the change in the number of solvent-exposed side-chain torsions or the total number of side chain torsions buried at the interface, and a constant contribution. Changes in the number of solvent-exposed main-chain torsions can also be counted for peptide ligands. It must be emphasized that theoretical and empirical considerations indicate that Eq. (1) will only produce accurate absolute binding affinity predictions for receptor–ligand reactions that approximate rigid-body association. Default values were used for each descriptor and all other important quantities. The model complex with the lowest empirical free energy score (most negative predicted absolute binding affinity) was ultimately selected as the best DR6–GFP NAPP structural interaction model. The refinement and scoring procedure was validated using the 1sg1 crystal structure (see Supporting Information).

Testing the DR6–GFD NAPP interaction model

Our modeling workflow allowed us to identify a single, physically realistic, DR6–GFD NAPP predicted complex structure. Importantly, our modeling workflow incorporated an extensive a priori testing to ensure the physical reasonableness and probable accuracy of the model. Our next task was to evaluate the accuracy of the docked model a posteriori.

Testing the DR6–GFD NAPP interaction model against the available biophysical data

Biophysical model testing began with a quantitative comparison between the theoretical binding affinity calculated from our model and an experimental estimate of the binding affinity. A similar validation calculation was performed on the p75–NGF interaction (see Supporting Information). Biophysical model testing also involved the analysis of pairwise sequence alignments between GFD NAPP and the N-terminus of APLP2 [Amyloid beta (A4) precursor-like protein 2], on the one hand, and DR6 and p75, on the other, because Nikolaev *et al.* showed that an N-terminal fragment of APLP2 binds to DR6 and that p75 binds to NAPP. Given this, we used structural superposition to model the p75–NAPP interaction and compared a theoretical estimate of the binding affinity with the experimental value (see Supporting Information). Finally, a comparison was made between the GFD NAPP interface residues implied by our model and the GFD NAPP interface residues suggested by the 22C11 antibody data.

Testing the DR6–GFD NAPP interaction model against the available theoretical data

The theoretical testing involved a comparison between the interface residues derived from our docked model with predicted binding site or interface residues for GFD NAPP and DR6, respectively, which were calculated using the protein–protein interaction prediction server (PPI-Pred; http://bmbpcu36.leeds.ac.uk/ppi_pred/overview.html).[39] From the coordinates of a monomeric protein structure, PPI-Pred typically predicts two or three binding patches or two or three well-defined residue patches that serve as protein–protein interaction sites. In the case of GFD NAPP, PPI-Pred produced two patch predictions (I and II); in the case of the DR6 ectodomain, three predicted interface patches were generated (I, II, and III). The PPI-Pred testing procedure was validated using the 1sg1 crystal structure (see Supporting Information).

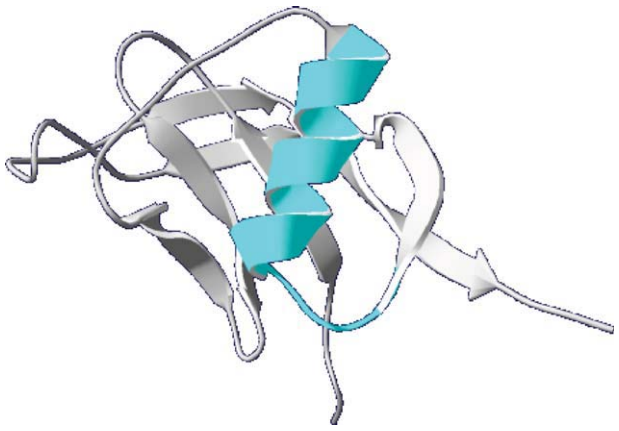

Figure 1

Ribbon representation of the GFD NAPP crystal structure with key residues highlighted. The PDB identifier for the structure is 1mwp. The structure comprises residues 28-123 and was solved at 1.8 Å resolution; the structure has an R-value = 0.203 and an R-free value = 0.242. The alpha helix and loop span residues 66-81 and makes up the known binding epitope for the anti-GFD NAPP antibody 22C11. Importantly, the 22C11 antibody is known to interfere with DR6-GFD NAPP binding. Hence, it is reasonable to assume that the same helix-loop motif makes up a key recognition element for DR6-GFD NAPP binding. Importantly, according to our best docked model GFD NAPP residues E67, G68, L70, Q71, Q74, P78, and E79 are all predicted to be interface residues. [Color figure can be viewed in the online issue, which is available at wileyonlinelibrary.com.]

RESULTS

The primary aim of this study was to construct a theoretical model of the DR6–GFD NAPP interaction, an interaction that may have implications for AD. A DR6–GFD NAPP interaction model was constructed using homology modeling, rigid-body docking, and free energy scoring. Calculations and model predictions were compared, to the extent permitted by the available data, with experimental results and independently generated theoretical results. The final model was analyzed to suggest the physical basis of DR6–GFD NAPP recognition, especially within the context of known TNFR interactions; some biophysical and biological implications suggested by the model are also considered.

Modeling and evaluating our refined DR6 homology model and the GFD NAPP crystal structure

Figure 1 provides a ribbon representation of the GFD NAPP crystal structure (28–123). GFD NAPP is a high-resolution high-quality crystal structure that exhibits a globular fold. Several key residues (66–81) that comprise a lone alpha-helix-loop motif are highlighted in cyan. Anti-GFD NAPP antibody 22C11 interacts with the alpha-helix-loop motif and blocks DR6–GFD NAPP binding. There is a good reason to conclude that the GFD NAPP crystal structure approximates a binding competent conformation.

Figure 2 provides a ribbon representation of our energy-optimized or -refined DR6 ectodomain homology model. The ectodomain of DR6 comprises residues 67–211. The model was constructed using the bound coordinates of the p75 receptor and probably represents a binding competent conformation. The DR6 ectodomain model takes on a more extended shape and exhibits beta secondary structure interconnected through less well-defined structural elements. The DR6 structure appears to form a structural depression or basket region that seems well suited to accommodate a globular protein such as GFD NAPP. The DR6 homology model was evaluated using a variety of computational tools, and the results are summarized in Table I. The refined DR6 homology model was ultimately docked to the GFD NAPP crystal structure.

Modeling the interaction between DR6 homology and GFD NAPP

Figure 3 provides a ribbon representation of the final or best DR6–GFD NAPP interaction model (model 1). The model indicates an important recognition role for the GFD NAPP alpha-helix-loop motif (residues 66–81). It also appears that the GFD NAPP alpha helix (66–76) rests in or lines the previously mentioned DR6 structural depression or basket. Worth noting is that the empirically calculated binding affinity of the best docked model (−11.1 kcal/mol) is in excellent agreement with the experimentally estimated binding free energy (−11.5

Figure 2

Ribbon representation of the refined DR6 ectodomain homology model. The refined DR6 ectodomain (67–211) homology model was built using the I-TASSER modeling server and was subject to energy minimization using a molecular mechanics energy function and GB/SA implicit solvent model.

Table I
We Built a DR6 Ectodomain (67-–211) Homology Model Using the I-TASSER Server

Model quality	DR6 I-TASSER model	Minimized DR6 I-TASSER model	p75 template structure (1sg1)
I-TASSER *C*-score[a]	1.31	N/A	N/A
I-TASSER TM-score[a]	0.9	N/A	N/A
I-TASSER RMSD[a]	2.2	N/A	N/A
ProSA *Z*-score[b]	−3.87	−4.33	−4.33
QMEAN score[c]	0.530	0.454	0.441
DFIRE energy[d]	−109.80	−124.85	−126.03
Minimization energy[e]	N/A	−4564.22	N/A

The model was optimized using implicit solvent energy minimization. The structural and physical quality of each I-TASSER model was evaluated using a variety of internal (I-TASSER) and external (ProSA, QMEAN, and DFIRE) tools.
[a]I-TASSEER server http://zhanglab.ccmb.med.umich.edu/I-TASSER/.
[b]ProSA Server https://prosa.services.came.sbg.ac.at/prosa.php.
[c]Qmean Server swissmodel.expasy.org/qmean/.
[d]http://swissmodel.expasy.org/workspace/.
[e]TINKER GB/SA AMBER99 minimization (kcal/mol).
The model quality assessment method is provided in column 1. Columns 2, 3, and 4 refer to the raw I-Tasser DR6 ectodomain homology model, the minimized DR6 ectodomain homology model, and the p75 ectodomain template structure. *C*-score values range from −5 to 2, with a higher value indicative of a good model. A TM-score > 0.5 is associated with a model of correct overall topology. A calculated RMSD value of 2.2 Å suggests a model with relatively high resolution. ProSA, Qmean, and DFIRE calculations can be used to assess model quality. ProSA, Qmean, and DFIRE values were calculated for the DR6 homology model, the optimized DR6 model, and for the p75 template structure (from 1sg1). The comparative ProSA, Qmean, and DFIRE scores all suggest a high-quality DR6 model. More detail is available in the text. The DR6 model was ultimately refined using energy minimization along with the Amber99 force field and GB/SA implicit solvent model, as implemented in the TINKER molecular modeling package. The model assessment data suggests that the optimized DR6 model is the best and most accurate model.

kcal/mol). Also provided are the calculated binding affinity values for the other nine ClusPro models and the amount of structural deviation between each of them and model 1, the best ClusPro model.

Biophysical testing of the DR6-GFD NAPP interaction model

Both NAPP and an N-terminal fragment of APLP2 have been shown to bind the DR6 ectodomain. Given this, we judged it worthwhile to align the sequences between GFD NAPP and APLP2. Figure 4 displays the sequence alignment; secondary structural information is also presented. The anti-GFD NAPP (22C11) antibody binding epitope is indicated by a solid black line. The GFD NAPP binding site residues suggested by our docking study were compared with the GFD NAPP binding site residues suggested by the experimentally observed inhibitory activity of the anti-GFD NAPP 22C11 antibody. The results are graphically summarized in Figure 5. Nikolaev et al. showed that the neurotrophin receptor p75 binds NAPP, albeit with lower affinity (−9.0 kcal/mol) than DR6. Given this, Figure 6 provides the results of a sequence alignment between the DR6 and p75 ectodomains. Also provided in Figure 6 is secondary structural information for DR6.

Theoretical testing of the DR6-GFD NAPP interaction model

PPI-Pred was used to predict binding patches for GFD NAPP and the ectodomain of DR6. For GFD NAPP, PPI-Pred produced two patches (I and II). For DR6, PPI-Pred calculated three binding patches (I, II, and III). The results for GFD NAPP are graphically summarized in Figure 5. Running from left to right (a, b, and c) are structural models that depict (in cyan) interface residues derived from the 22C11 antibody binding experiments, putative GFD NAPP interface residues derived from the present docking study, and potential interface residues obtained from the PPI-Pred calculations. Only the calculated PPI-Pred residues that agree with the residues obtained from docking study are shown. The results are also summarized in Table II. As in the case of GFD NAPP, putative DR6 interface residues derived from the docking study were compared with potential DR6 interface residues derived from PPI-Pred. Unlike the case with GFD NAPP, an experimentally derived DR6 interface residue set proved to be unavailable. Only the calculated PPI-Pred residues that agree with the residues obtained from docking are shown. The results are summarized in Figure 7 and in Table III.

The interface interactions suggested by our DR6-GFD NAPP interaction model

The DR6–GFD NAPP interface suggested by our model is characterized by four salt bridges and seven hydrogen bonds. The favorable salt bridge contribution to binding is partially offset by the two charged groups that undergo complete burial at the interface. The interface is further characterized by the burial of some 43 hydrophobic groups, the immobilization of 35 side chain torsions, and a gap volume of 4289 $Å^3$. Importantly, all descriptor values are within normal ranges for crystal structures.[19] The relevant data is summarized in Figure 8 and Tables IV–VI.

DISCUSSION

According to the developmental model of Nikolaev et al., NAPP binding to the DR6 ectodomain causes accelerated neuronal apoptosis and axonal degeneration through the downstream action of caspase-3 and caspase-6. By this mechanism, neuronal connections are sculpted during development; it is hypothesized that this pathway is highjacked in the AD brain.

The structural details that characterize the DR6–NAPP interactions are unclear. In an effort to elucidate some of those details, we produce a model of the DR6–NAPP interaction through the use of homology modeling, rigid-body docking, implicit solvent energy optimization, and free energy scoring. Our work-flow converged on a single physically plausible model (model 1).

A

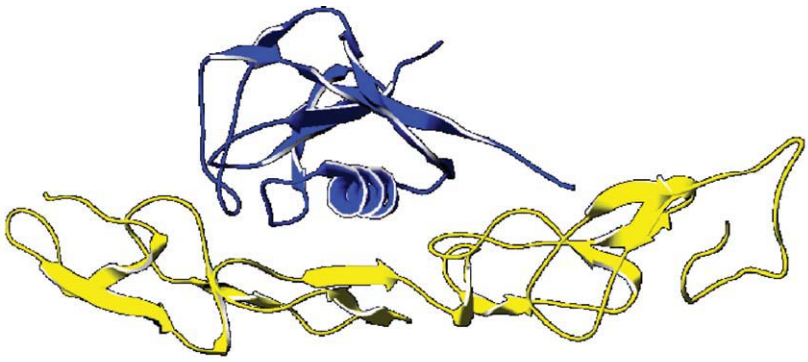

B

DR6-GFD NAPP Complex model	$\Delta G_{bind,empirical}$ (kcal/mol)	$\Delta G_{bind,exp}$ (kcal/mol)
1 (best one)	-11.1	-11.5

C

DR6-GFD NAPP Complex model	$\Delta G_{bind,MM-GB/SA}$ (kcal/mol)	$\Delta G_{bind,empirical}$ (kcal/mol)	RMSD (Å)
1 (best one)	-20.5	-11.1	0
2	-2.5	-3.3	16.3
3	4.4	-1.8	19.8
4	> 10.0	-5.3	11.6
5	-39.1	-5.6	12.4
6	-24.3	6.2	9.1
7	-32	-3.6	11.4
8	-17.6	-3.9	20.5
9	1.8	-3.3	27.5
10	-9	0.7	20.4

Figure 3

Ribbon representation and binding affinity values for best DR6–GFD NAPP interaction model and the top 10 interaction models. (A) The refined DR6 ectodomain (67–211) homology model was docked to the GFD NAPP crystal structure using the rigid-body ClusPro protein–protein docking server. The model clearly reveals an important recognition role for the lone GFD NAPP alpha helix, in good agreement with the 22C11 antibody data (see Figs. 1 and 4 for more details). According to our methodology, the top 10 ClusPro models were selected for further analysis. All 10 ClusPro complexes were subject to rigid-body energy minimization and scored using a standard MM-GB/SA methodology. Complexes with negative MM-GB/SA binding free energies were then scored using our own empirical free energy function [Eq. (1)]. (B) The ClusPro model with the best empirical binding free energy [most negative predicted binding affinity using Eq. (1)] was selected as the best complex model and is displayed above. The predicted binding affinity (−11.1 kcal/mol) for the best ClusPro model compares favorably with an experimentally derived estimate for the DR6–NAPP binding affinity (−11.5 kcal/mol). The experimentally derived estimate for the binding affinity is based on a reported EC50 of 4.6 n*M*. (C) The refined DR6 ectodomain (67–211) homology model was docked to the GFD NAPP crystal structure using the rigid-body ClusPro protein–protein docking server. According to our methodology, the top 10 ClusPro models were selected for further analysis. All 10 ClusPro complexes were subjected to rigid-body energy minimization and scored using a standard MM-GB/SA methodology. Complexes with negative MM-GB/SA binding free energies were then scored using an empirical free energy function [Eq. (1)]. The complex with the best empirical binding affinity was selected as the best model and was retained for further analysis (model 1). The average structural deviation of each ClusPro complex with respect to the best ClusPro complex is also provided. The RMSD results clearly indicate the structural uniqueness of each complex. The deep and physically plausible free energy minimum of model 1 suggests it is a high-quality docked model of probable accuracy. [Color figure can be viewed in the online issue, which is available at wileyonlinelibrary.com.]

Nikolaev *et al.* performed binding experiments, which indicate that among the TNFR receptors tested, NAPP only binds DR6 and p75. It binds DR6 with low nanomolar affinity (EC50 $\approx$ 4.6 n*M* or $\Delta G_{bind,exp} \approx -11.5$ kcal/mol) and p75 with weaker affinity (EC50 $\approx$ 300 n*M* or $\Delta G_{bind,exp} \approx -9.0$ kcal/mol). Additional biophysical evidence presented by Nikolaev *et al.* indicates that APLP2 binds DR6 and suggests that the growth factor domain of NAPP (GFD NAPP) is the primary DR6 ectodomain interaction partner. In particular, the fact that

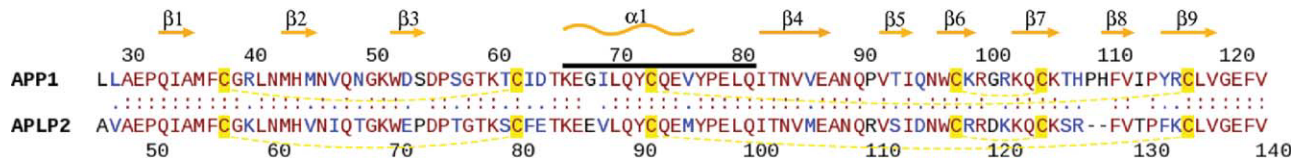

Figure 4

Sequence alignment and secondary structure of the growth factor-like domain of human N-terminal APP (GFD NAPP) and APLP2. Disulfide bonds are shown as dash lines, identical residues are connected by two dots, conserved residues - by a single dot, and non-conserved residues have no connection. The alignment was performed via the LALIGN server (http://www.ch.embnet.org/software/LALIGN_form.html). Both NAPP and an N-terminal fragment of APLP2 have been shown to bind the DR6 ectodomain. Thus, given the reasonable assumption that binding motifs are highly conserved between protein ligands that bind to the same receptor, we aligned the two sequences and calculated percent identify and similarity scores. For the global alignment the percent identity and the percent similarity were calculated to be 71% and 93%, respectively. Using the ClusPro predicted interface residues (identified according to a 4.5 Å cutoff) for GFD NAPP and the corresponding aligned positions for APLP2, the percent identity and similarity were calculated to be 76% and 92%, respectively. Keeping in mind that such an analysis suffers from some uncertainty, the alignment data can be plausibly interpreted in support of our docked DR6-GFD NAPP model. The anti-GFD NAPP (22C11) antibody binding epitope is indicated by a solid black line. Nikolaev and co-workers showed that 22C11 blocks the interaction between DR6 and GFD NAPP. Thus, it is reasonable to assume that the DR6-GFD NAPP interaction, at least in part, is mediated by some of the same residues that comprise the 22C11 binding epitope. And, this appears to be the case (see other Figures, Tables and text for further details). [Color figure can be viewed in the online issue, which is available at wileyonlinelibrary.com.]

the GFD NAPP antibody 22C11 blocks NAPP binding to DR6 provides strong evidence that GFD NAPP provides the primary or even exclusive interaction surface for the DR6–NAPP interaction.

Importantly, a high-resolution crystal structure of GFD NAPP (28–123) is available. Unfortunately, a DR6 ectodomain structure is lacking. Nevertheless, we were able to make progress toward our ultimate goal by constructing an optimized DR6 homology model; both structures appear to represent binding competent conformations. This is important because studies indicate that modeling protein–protein complexes from binding competent or bound conformations produces more accurate modeling results.[14,15,37,38,40–42] The optimized DR6 ectodomain model was subsequently docked to the GFD NAPP crystal structure and model 1 was ultimately selected as the best model, according to an empirical estimate of the binding affinity. Model 1 was then compared against the available biophysical data and independently generated theoretical data. The evidence suggests that our DR6–GFD NAPP model is roughly accurate and captures

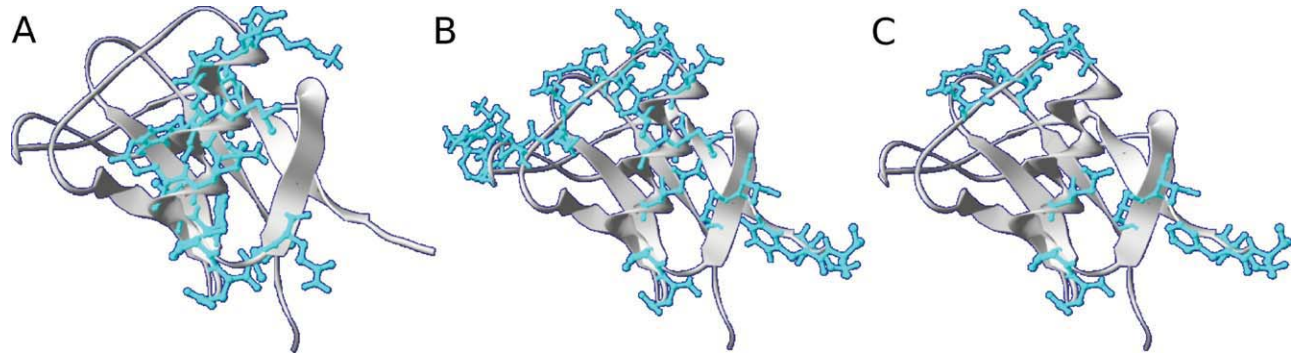

Figure 5

Ribbon representations of GFD NAPP along with 22C11, ClusPro predicted, and PPI-Pred predicted interface residues. Using a crystal structure of GFD NAPP (1mwp) and a refined homology model of the DR6 ectodomain, we constructed a structural model of their interaction using the ClusPro docking server. We then compared the predicted ClusPro interface residues with the binding epitope of the 22C11 anti-GFD NAPP antibody that is known to block binding to the DR6 ectodomain. We also compared the ClusPro residues with interface residue predictions generated using the protein-protein interaction prediction server (PPI-Pred). In the case of GFD NAPP, PPI-Pred produced two predicted binding patches (I and II). The above displayed residues were derived from both patches; only PPI-Pred residues that agree with the ClusPro residues are displayed. We reasoned that overlap between all three disparate residue sets would tend to verify our model; this appears to be the case. (A) Ribbon representation of GFD NAPP along with the 22C11 antibody binding epitope residues shown as "balls-and-sticks". (B) Ribbon representation of GFD NAPP along with ClusPro predicted interface residues shown as "balls-and-sticks". A residue was identified as a ClusPro interface residue according to a 4.5 Å inter-chain distance criterion. (C) Ribbon representation of GFD NAPP along with PPI-Pred predicted interface residues shown as "balls-and-sticks". The PPI-Pred residues were derived from PPI-Pred predicted patches (I and II) and only residues that overlap with the ClusPro residues are displayed. [Color figure can be viewed in the online issue, which is available at wileyonlinelibrary.com.]

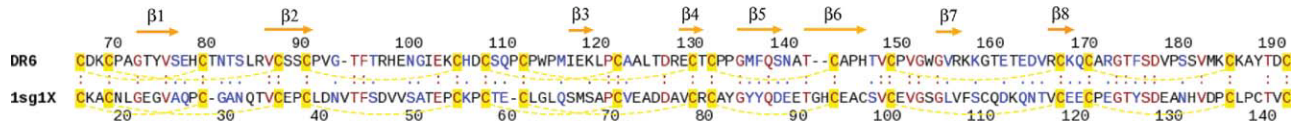

Figure 6

Sequence alignment and secondary structure of the human DR6 ectodomain and its homolog, p75 (1sg1, chain X). The alignment was calculated using the LALIGN server. Disulfide bonds are shown as dashed lines, identical residues are connected by two dots, conserved residues - by a single dot, and non-conserved residues have no connections. The basic logic for using the alignment to test our DR6-GFD NAPP protein-protein interaction model is described in the text and is summarized in Fig. 1. For the global alignment, the percent identify was calculated to be 30% and the percent similarity was calculated to be 54%. For the ClusPro predicted interface residues, the values were calculated to be 27% and 36%, respectively. The results of this analysis, while arguably inconclusive, suggest that the relatively poor sequence conservation can account for the reduced affinity of NAPP for p75. This inference is further supported by a structural model of the p75-GFD NAPP interaction (see Supplementary Information). [Color figure can be viewed in the online issue, which is available at wileyonlinelibrary.com.]

the essential structural details of DR6 binding to NAPP and that the model can be used to rationalize results and suggest testable ideas and future experiments.

The GFD NAPP crystal structure is a high-quality binding competent structure

We were able to locate two NAPP crystal structures. One structure (3ktm) had a crystallographic resolution of 2.7 Å, spanned residues 23–202, and provided the homodimerized or bound coordinates of NAPP. The second structure (1mwp) is a higher resolution (1.8 Å) crystal structure that specifically includes residues 23–128 of the GFD domain. The superior *R*-value (0.203), *R*-free value (0.242), and unblemished Ramachandran plot (data not shown) of the 1mwp GFD NAPP structure further indicate a structure that is better suited for modeling work. Moreover, structural superposition revealed that the Ca atoms of the unbound 1mwp crystal structure are almost identical with the common Ca atoms of the bound 3ktm NAPP structure (≈1.2 Å rmsd). Thus, 1mwp was selected as providing a high quality and binding competent GFD NAPP structure for rigid-body docking to the DR6 ectodomain. As indicated in Figure 1, the 1mwp GFD NAPP structure reveals a predominantly beta globular structure with a single alpha helical-loop segment that spans residues 66–81. As discussed below, this alpha helix-loop motif, particularly the alpha helix (66–76), appears to play an important role in DR6–GFD NAPP recognition.

The p75 receptor crystal structure is a high-quality binding competent structure that provides a good template for building a high-quality binding competent DR6 ectodomain homology model

The 1sg1 crystal structure contains the coordinates of a 2:1 complex between NGF and p75. The structure is a reasonably high quality structure with good resolution (2.40 Å), an acceptable *R*-value (0.245) and an acceptable *R*-free value (0.269). With the exception of Asp112, all nonglycine residues are located within the allowed regions of the Ramachandran map (data not shown). Like DR6, the p75 receptor is a member of the TNFR family; it is known to bind NAPP with high nanomolar affinity. Like DR6, the p75 receptor appears to play a role in apoptosis and has been implicated in AD. The overall sequence coverage between p75 and DR6 includes the entire DR6 ectodomain (67–211), with a sequence identity of ≈28%. Clearly, the p75 structure represents a binding competent conformation. Moreover, the 1sg1 p75 structure can be superimposed to within ≈1.2 Å Ca rmsd onto a second p75 receptor crystal structure that was solved in complex with neurotrophin-3 (PDB code: 3buk).[43] Despite the low overall rmsd value, the structural superposition revealed significant flexibility for the first 15 N-terminal residues of p75. Nevertheless, the 1.2 Å rmsd result suggests that the binding competent conformations of p75 and similar receptors, such as

Table II

Comparisons between Three Different Methods for Predicting Interface Residues for GFD NAPP

ClusPro -predicted interface residues for GFD NAPP: C38,G39,T59,K60,T61,C62,I63,D64,T65,E67,G68,L70,Q71,Q74,P78,E79,I82, T83,K99,R100,K103, Q104,E121,F122,V123
PPI-Pred-predicted interface residues for GFD NAPP: C38,G39,T61,C62,I63,D64,T65,Q74,P78,E79,I82,T83,E121,F122,V123
22C11 -predicted interface residues for GFD NAPP: K66,E67,G68,I69,L70,Q71,Y72,C73,Q74,E75,V76,Y77,P78,E79,L80,Q81

The first row provides the interface residue predictions or contributions of GFD NAPP implied by our DR6–GFD NAPP ClusPro-docked model, using a 4.5-Å interchain cutoff criterion. The residues provided in the first row provide the basis for comparison with the bottom two rows. Residue agreement with the first row is thus indicated by underlining residues in the bottom two rows. Substantial agreement between the three independently generated data sets would tend to verify our docked model and this appears to be the case.The second row provides interface residue predictions for GFD NAPP that were generated using PPI-Pred. Only PPI-Pred residues that agree with the ClusPro residues are shown. For GFD NAPP, PPI-Pred predicted two binding patches (I and II). Patch I has 25 residues; eight overlap with the ClusPro interface residues; the first eight residues above correspond to patch I. Patch II has 19 residues; seven overlap with the ClusPro residues; the last seven residues are from patch II. The third row provides interface residue predictions for GFD NAPP that were inferred from the fact that (1) the anti-GFD NAPP antibody 22C11 has a known GFD NAPP binding epitope (displayed) and (2) that 22C11 blocks the interaction between DR6 and GFD NAPP. Thus, we assume or predict that to block the DR6 interaction 22C11 is binding to the very GFD NAPP epitope that, at least in part, mediates binding to DR6. Residues that agree with the ClusPro predictions are underlined.

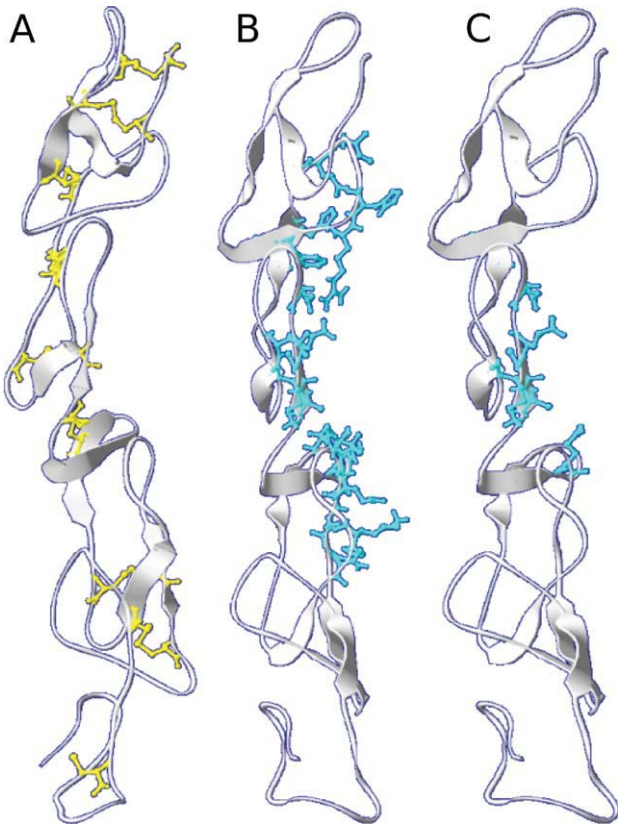

Figure 7

Ribbon representations of the DR6 ectodomain homology model along with ClusPro predicted and PPI-Pred predicted interface residues. See the text and Fig. 2 for more details. The presented data tends to verify our DR6-GFD NAPP model. (A) Ribbon representation of the DR6 ectodomain homology model structure. The structure was built using the I-TASSER modeling server. Cysteine residues are shown as "balls-and-sticks". (B) Ribbon representation of the DR6 ectodomain along with ClusPro predicted interface residues depicted as "balls-and-sticks". (C) Ribbon representation of the DR6 ectodomain along with PPI-Pred predicted interface residues depicted as "balls-and-sticks". The PPI-Pred residues were derived from PPI-Pred predicted patches (I, II and III) and only residues that overlap with the ClusPro residues are displayed. [Color figure can be viewed in the online issue, which is available at wileyonlinelibrary.com.]

DR6, probably sample a narrow range of conformations and that a single binding competent DR6 structure is probably suitable for a rigid-body docking study. These familial, structural, biophysical, and biological considerations strongly suggest that p75 is a good template for constructing a high-quality structural model of the binding competent conformation of the DR6 ectodomain.

Our refined DR6 ectodomain homology model structure is a high-quality binding competent structure

An experimentally determined DR6 structure is currently unavailable. Thus, we decided to construct a homology model of the DR6 ectodomain using residues 67–211 and the I-TASSER modeling server (Fig. 2). Multiple lines of evidence suggest that our I-TASSER DR6 ectodomain homology model is an accurate one that is suitable for modeling work and, in particular, for rigid-body docking to the GFD NAPP crystal structure.

First, and as described above, the p75 receptor that served as the template for our DR6 ectodomain model represents a binding competent conformation and is a good template structure. These considerations alone suggest that a binding competent model of the DR6 ectodomain can be constructed to within <2.0 Å Ca rmsd of the bound DR6 structure that will someday be revealed by experiment.[44,45]

Second, we built our DR6 model using the I-TASSER server, a homology modeling server that has been widely used by the scientific community and that was ranked first in both the CASP7 and CASP8 experiments. The I-TASSER server follows an especially demanding computational workflow. In particular, I-TASSER automatically selects appropriate protein template structures and builds a model of the target or query structure (DR6) through a rigorous procedure that involves fragment reassembly of aligned regions, *ab initio* model construction of unaligned regions, clustering, energy scoring, and optimization of the target structures hydrogen bonding network. These historical and methodological considerations further suggest the physical accuracy and reliability of our final DR6 ectodomain model.

Third, the internal quality checks automatically calculated by the I-TASSER server further suggest that our DR6 ectodomain model is an accurate one. In particular, for the top-ranked model, the I-TASSER server calculates a *C*-score, a predicted TM-score and a predicted RMSD value. Briefly, the *C*-score represents a confidence score for estimating the overall quality of a model. Typically, *C*-score values are in the range of -5 to 2, with a higher value indicative of a model with high confidence. The *C*-score of our DR6 model is on the higher side of that range (1.31), which suggests a high confidence model. The target TM and RMSD values provide quantitative estimates of how much the I-TASSER homology model is predicted to structurally deviate from a hypothetical crystal structure. A TM score > 0.5 indicates a model of correct topology and an RMSD < 0.9 would indicate a model that is predicted to be within the unavoidable error of a crystal structure. The TM-score (0.9 ± 0.06) and RMSD value (2.2 ± 1.7) calculated for our DR6 model thus indicate a very good model that is well-suited for further modeling work. The results of the I-TASSER quality analysis are summarized in Table I.

Fourth, in addition to the internal I-TASSER quality checks, we calculated additional quality checks using three independent server-based methods (ProSA, Qmean, and DFIRE). All three methods provide independent verification that our DR6 homology model is a reasonably

Table III
Comparisons between Two Different Methods for Predicting Interface Residues for the Homology Model of the DR6 Ectodomain

ClusPro-predicted interface residues for DR6 ectodomain homology model:
F96,R98,H99,I103,E104,H107,D108,K120,L121,D128,E130,C131,T132,Q139,N141,A142,K158,E162,T163,E164,D165,R167
PPI-Pred -predicted interface residues for DR6 ectodomain homology model
D108,K120,D128,E130,C131,T132,Q139

PPI-Pred produced three patch predictions for DR6. Only PPI-Pred predictions that agree with the ClusPro residues are shown. For DR6, PPI-Pred produced three patch predictions (I, II, and III). Patch I has 27 residues, Patch II has 31 residues, and patch III has 17 residues. All of the above displayed PPI-Pred residue predictions are derived from Patch II. More details are provided in the text and in Table I. The good agreement exhibited between the two interface residue data sets tends to verify our DR6–GFD NAPP docked interaction model.

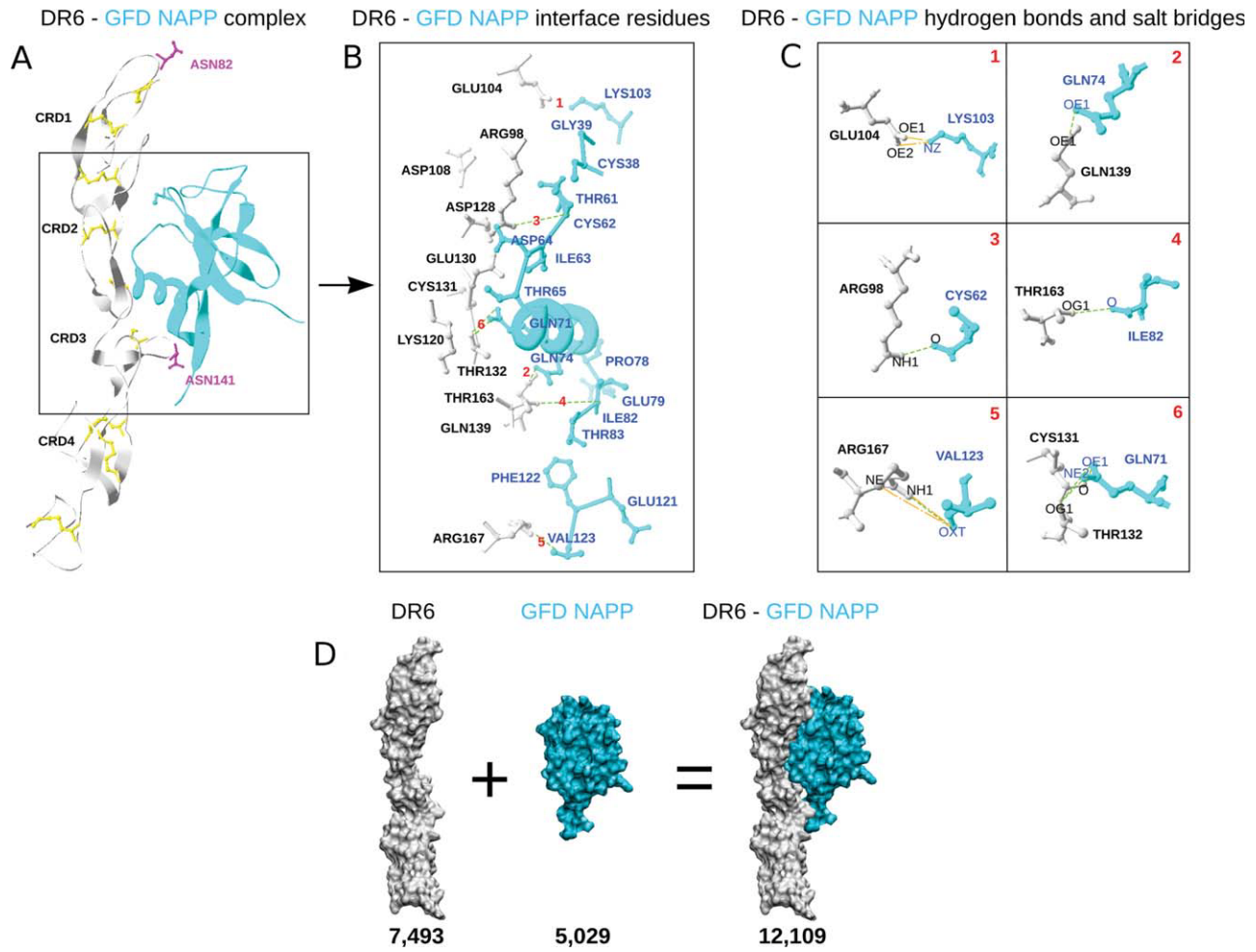

Figure 8
Final DR6–GFD NAPP-docked structure showing important interface residues, sites of glycosylation, and the rigid body docking association of the complex. (A) Final structure of the DR6–NGF NAPP complex. Cysteine rich domains (CRD) are shown in black bold font, cysteine residues are represented by yellow balls-and-sticks, and sites of glycosilation are labeled and represented by pink balls-and-sticks. (B) DR6–NGF NAPP interface. Backbone is represented by carbon alpha trace. DR6 residues have black labels, whereas GFD NAPP residues are labeled blue. Hydrogen bonds are shown as green dash lines. Specific interactions are enumerated and shown in greater detail in C). (C) Interface hydrogen bonds and salt bridges (see also Tables V and VI). Hydrogen bonds are shown as green dash lines, salt bridges—as orange dash dot lines. Box 1: Interaction between residue GLU104 of DR6 and LYS103 of GFD NAPP. Box 2: Interaction between residue GLN139 of DR6 and GLN74 of GFD NAPP. Box 3: Interaction between residue ARG98 of DR6 and CYS62 of GFD NAPP. Box 4: Interaction between residue THR163 of DR6 and ILE82 of GFD NAPP. Box 5: Interaction between residue ARG167 of DR6 and VAL123 of GFD NAPP. Box 6. Interaction between residues CYS131 and THR132 of DR6 and GLN71 of GFD NAPP. (D) Rigid body association of the DR6–NGF NAPP complex. Molecules are represented by solvent accessible surface areas (SASA) with numbers given in $Å^2$.

Table IV
Physical Descriptors and Individual Binding Free Energy Contributions for the Best Predicted DR6-–GFD NAPP Interaction

Physical descriptor (type)	Physical descriptor (quantity)	Free energy contribution (kcal)
$-0.79\Delta X_{+/-}$	−2	1.58
$0.075\Delta X_{c/s}$	−43	−3.23
$-0.65X_{sb}$	4	−2.6
$-0.86X_{hb}$	7	−6.02
$-0.089\Delta X_{tor}$	−37	3.29
$-0.00089X_{gap}$	4375	−3.89

Equation (1) was used to calculate all predicted binding affinities (kcal/mol). In particular, Eq. (1) was validated by being used to accurately calculate the binding affinity of the p75-NGF interaction (see Supporting Information) and was used to calculate predicted binding affinities for the ten 10 energy-optimized ClusPro models. Physical descriptor values and individual binding free energy contributions for the best DR6–GFD NAPP-docked model are provided in the table. The predicted binding affinity for the best DR6–GFD NAPP model was calculated to be −11.1 kcal. The various physical descriptors that contribute to Eq. (1) and their regression-derived weights are listed in column 1. From the top down, the weighted physical descriptors are (1) the change in the number of solvent-exposed charged groups, (2) the change in the number of solvent-exposed hydrophobic groups (carbon and sulfur atoms), (3) the number of interface salt bridges, (4) the number of interface hydrogen bonds, (5) the change in the number of solvent-exposed side chain torsions, and (6) the interface gap volume. Not shown is a −0.33 kcal constant contribution. Column 2 lists the actual descriptor counts and values calculated from the ClusPro-generated and energy -optimized coordinates of what we identified as the best docked DR6–GFD NAPP model. The units for the gap volume descriptor are $Å^3$. Column 3 lists the individual free energy contributions implied by the various regression-weighted descriptors. A negative value implies a favorable contribution to binding, while whereas a positive value implies and unfavorable contribution to binding.

accurate one. The ProSA server calculates an overall *z*-score that can be used to evaluate the structural quality of a computational protein model with respect to crystal structures and NMR structures. The Qmean server uses a five-term composite scoring function that includes a torsional potential, a pairwise interaction potential, a solvation term, and two terms that quantify the level of agreement between predicted secondary structure and residue accessibilities and observed model secondary structure and residue accessibilities. The Qmean server outputs a pseudo-energy that can be used to asses model quality; the lower the calculated Qmean score the better. DFIRE is an all-atom statistical potential that can be used to assess nonbonded interactions in a given protein model. A pseudo-energy for the entire model is provided, which reflects the quality of the model. A lower energy indicates a more native-like model. The results from the ProSA, Qmean, and DFIRE calculations are provided in Table I and clearly indicate that our DR6 ectodomain model, especially when compared with the corresponding 1sg1 p75 receptor template structure values, is physically reasonable and is useful for further modeling work and analysis.

Finally, we attempted to refine and improve our DR6 model through energy minimization with an implicit solvent model. The problem of refining reasonably good homology models is a difficult but important one. Recent work by Summa and co-workers suggests that energy minimization using an all-atom molecular mechanics force field or knowledge-based potential, especially when combined with an implicit (GB/SA) solvent model, can be used to improve the structural agreement between model structures and crystal structures.[46–48] In particular, their work suggests that energy minimization combined with an implicit treatment of the solvent can be used to hold crystal structures in their native conformations and move decoy structures into better agreement with crystallographic ones. Given this, we energy minimized our DR6 ectodomain homology model using the Amber99 force field and GB/SA implicit solvent model, as implemented in the TINKER molecular modeling package. Against the backdrop of the results of Summa, Chopra, and Levitt, the successful convergence of the minimization and the extremely low relative conformational free energy (−4564.2 kcal/mol) suggests that the minimization resulted in a superior DR6 model. Moreover, Qmean, ProSA, and DFIRE calculations on the refined DR6 model further suggest its generally improved structural and physical quality. The results are summarized in Figure 2 and Table I. In summary, we have good reason to conclude that our energy minimized homology model represents a reasonably accurate and high quality model of the binding competent conformation of the DR6 ectodomain.

Table V
Interface Salt Bridges for the Best Predicted DR6–GFD NAPP-Docked Model

A	B	Distance (Å)
Glu 104 OE1	Lys 103 NZ	3.57
Glu 104 OE2	Lys 103 NZ	2.97
Arg 167 NE	Val 123 OXT	3.73
Arg 167NH1	Val 123 OXT	2.91

Column A refers to the DR6 homology model (receptor) and column B refers to the GFD–NAPP crystal structure (ligand). A salt bridge is defined as an interaction between two charged atoms that are separated by 4.0 Å or less.

Table VI
Interface Hydrogen Bonds for the Best Predicted DR6–GFD NAPP-Docked Model

A	B
Cys 131 O	Gln 71 OE1
Thr 132 OG1	Gln 71 NE2
Thr 132 OG1	Gln 71 OE1
Gln 139 OE1	Gln 74 OE1
Arg 98 NH1	Cys 62 O
Thr 163 OG1	Ile 82 O
Arg 167 NH1	Val 123 OXT

Column A refers to the DR6 homology model (receptor) and column B refers to the GFD–NAPP crystal structure (ligand). Hydrogen bonds were identified according to the "Levitt" criteria, as implemented in the hydrogen bond detection program of Mark Gerstein; the program is available as part of the "Libproteingeometry" distribution and is available at the Gerstein lab page (http://geometry.molmovdb.org/files/libproteingeometry/src-prog2/README.html). The same program is used to calculate the hydrogen bond descriptor of Eq. (1). Because of the difficulty of distinguishing nitrogen from oxygen atoms, Gln and Asn epsilon (OE1) and delta (OD1) oxygen atoms are counted as hydrogen bond donors and acceptors, respectively.

The ClusPro rigid-body docking server can be used to accurately model the DR6–GFD NAPP interaction

A guiding postulate of this study is that the use of binding competent conformations along with rigid-body docking will produce superior protein–protein complex predictions than the use of unbound conformations. This postulate is consistent with the results of previous rigid-body docking studies. Thus, there is good reason to think that rigid-body docking can be used to produce a reasonably accurate DR6–GFD NAPP complex model.

To predict the DR6–GFD NAPP complex interaction, we specifically used rigid-body docking using the ClusPro server. ClusPro was selected because of the long and rigorous publication history that underlies its basic methodology, its accessibility and ease of use, its widespread use by structural biologists, and its impressive record of success in the CAPRI competitions.[14,37,38,40,41] Our own ClusPro validation study on the p75–NGF interaction resulted in a roughly accurate model of p75–NGF complex that was also ranked first (see Supporting Information). In all, the ClusPro server, in the case of rigid-body association, can be used to produce acceptable, native-like complex models with a >50% success rate. Thus, there is good reason to think that the ClusPro results for DR6–GFD NAPP docking produced at least one acceptable complex model that is suitable for further refinement and analysis.

The ClusPro DR6–GFD NAPP complex predictions can be further refined through rigid-body docking to produce an improved DR6–GFD NAPP interaction model

Following the ClusPro calculations, the top 10 docked models were subject to rigid-body energy minimization. Work in our laboratory and by other groups suggests that this protocol or similar protocols often results in more accurate complex structures and an enhanced ability to identify accurate or native-like protein–protein interactions (our data is unpublished).[49,50] In fact, rigid-body energy minimization for the best p75–NGF ClusPro model resulted in a dramatically improved model that almost perfectly aligned with the crystal coordinates of the p75–NGF complex (see Supporting Information). Thus, there is good reason to think that our rigid-body energy minimization protocol resulted in at least one roughly accurate DR6–GFD NAPP model complex that was significantly improved with respect to the raw ClusPro results.

The molecular mechanics-based and empirical free energy scoring can be used to identify the most accurate DR6–GFD NAPP complex

The top 10 energy optimized DR6–GFD NAPP ClusPro models were scored and ranked using a molecular mechanics potential and GB/SA implicit solvent model ($\Delta G_{bind,MM\text{-}GB/SA}$) and an empirical free energy function ($\Delta G_{bind,empirical}$). The empirical free energy expression is provided by Eq. (1). Previous work, including our own unpublished work, suggests that implicit solvent models, in particular GB/SA style models, and molecular mechanics energy functions, can be used to more accurately score and rank docked complexes.[49] According to our protocol, all energy-optimized ClusPro-docked complexes with $\Delta G_{bind,MM\text{-}GB/SA} > 0$ were filtered out as physically unrealistic and eliminated from further consideration. The absolute binding affinities of the selected models were then estimated using Eq. (1) ($\Delta G_{bind,empirical}$). Equation (1) can be used to accurately estimate the absolute binding affinity according to a regression-weighted sum of six physical descriptors, subject to the assumption of rigid-body association. The six descriptors include the number of hydrophobic and charged groups that are buried on complex formation, the number of buried interface salt bridge and hydrogen bonding interactions, the number of side chain torsions that are immobilized on binding and the interface void or gap volume. The function has been exhaustively tested and has been shown to have an accuracy of $\approx\pm 1.0$ kcal/mol and to be capable of correctly ranking native and native-like binding modes with respect to non-native ones. This rescoring and reranking protocol was successfully applied to the top 10 energy-optimized p75–NGF-docked models (see Supporting Information). Thus, the available data strongly suggests that the protocol can be used to identify the most accurate DR6–GFD NAPP model complex.

Our docking, rigid-body optimization, and free energy scoring workflow resulted in the identification of a single, structurally unique, and physically reasonable DR6–GFD NAPP interaction model of probable accuracy

Our docking, refinement, and free energy estimation protocol ultimately converged on a single DR6–GFD NAPP complex model (model 1) that was selected as the best model (Fig. 3). The final results suggest that model 1 is a good one for at least three reasons. First, model 1 is structurally distinct with respect to the other nine docked models. Second, it has a predicted binding affinity ($\Delta G_{bind,empirical} = -11.1$ kcal) that is significantly lower than the predicted binding affinity for the second best model ($\Delta G_{bind,empirical} = -5.6$ kcal). Third, in absolute terms the predicted binding affinity ($\Delta G_{bind,empirical} = -11.1$ kcal) is physically plausible. Thus, the best DR6–GFD NAPP model occupies a deep, structurally unique, and physically realistic free energy minimum with respect to the other nine ClusPro binding modes, and this suggests a physically and structurally realistic result or probable accuracy.

The best DR6–GFD NAPP complex model is suitable for further testing

The fundamental propriety of our homology modeling, rigid-body docking, refinement, rescoring, and

reranking procedure is strongly suggested by the prior work of others, by the results presented here, and by prior validation on the p75–NGF interaction (see Supporting Information). Thus, a priori considerations suggest that model 1 is of probable accuracy. The next step is to test model 1 a posteriori. In what follows, we divide the testing into two categories: (1) biophysical testing and (2) theoretical testing of the model. The biophysical model testing phase involved binding affinity comparisons, the analysis of GFD NAPP and DR6 sequence alignments and a comparative analysis with the available anti-GFD NAPP 22C11 antibody data. The theoretical model testing phase involved comparisons between data derived from our DR6–GFD NAPP model and independently generated computational data.

Our DR6-GFD NAPP complex model is verified by the available biophysical data

An experimentally based estimate of the binding affinity for the DR6–GFD NAPP interaction agrees almost perfectly with a theoretical estimate of the binding affinity derived from our DR6–GFD NAPP model (Fig. 3). This counts as impressive evidence that our model interface is a reasonable one. In particular, Nikolaev at al. used an ELISA-based technique to experimentally determine the strength of the DR6–NAPP interaction ($EC_{50} \approx 4.6$ n*M*). This provided us with the opportunity to compare the empirically predicted binding affinity implied by our DR6–GFD NAPP model [Eq. (1), $\Delta G_{bind,empirical} = -11.1$ kcal/mol] with the corresponding experimentally derived quantity ($\Delta G_{bind,exp} \approx -11.5$ kcal/mol). The observed level of agreement between theory and experiment is excellent and while it does not prove that our model is an accurate one, it nevertheless provides strong verification of our model. The results of this test are all the more impressive given that Eq. (1) was used to accurately calculate the binding affinity of the p75–NGF interaction (−11.8 kcal/mol predicted vs. −12.4 kcal/mol experimental) that served as the template for our DR6 homology model (see Supporting Information).

In addition to binding NAPP, Nikolaev *et al.* also showed that the DR6 ectodomain binds the N-terminus of APLP2 and with similar affinity. By making the reasonable assumption that APLP2 adopts a similar binding configuration to DR6 as does GFD NAPP, we can infer that a sequence alignment between APLP2 and the interface residues of GFD NAPP will reveal significant conservation. Thus, we compared the predicted interface residues of GFD NAPP, derived from our DR6–GFD NAPP model, with the aligned residue positions of APLP2. The alignment revealed that the GFD NAPP interface residues align almost perfectly with the APLP2 residues that probably mediate binding to DR6 (Fig. 4). This provides indirect evidence that the residue-level contribution of GFD NAPP to DR6 binding is captured by our model.

Nikolaev *et al.* also showed that the NAPP antibody 22C11 interferes with DR6–NAPP binding. Importantly, Hilbich *et al.* showed that the binding epitope recognized by the 22C11 antibody spans NAPP residues 66–81. This represents a stretch of residues that are localized around the lone helix (66–76) of GFD NAPP. On the assumption that 22C11 blocks DR6 binding to NAPP by binding to the same GFD NAPP surface that mediates DR6–GFD NAPP interaction, we compared the GFD NAPP interface residues derived from our model with the GFD NAPP epitope that is known to bind 22C11. Once again, we reasoned that good agreement between the two would tend to verify our model. Using a 4.5-Å cutoff criterion, the GFD NAPP residues that line the DR6–GFD NAPP interface of our model include residues 67, 68, 70, 71, 74, 78, and 79. Thus, there exists excellent agreement between the experimentally determined 22C11 epitope and the interface residues of our model. Thus, the modeled GFD NAPP contribution to DR6 binding enjoys further verification and, moreover, focuses attention on the specific role played by helix residues 66–76 in DR6–NAPP recognition.

In addition to binding DR6, Nikolaev et al. also showed that NAPP binds the p75 receptor, albeit with significantly reduced interaction strength. Thus, we attempted to align the p75 sequence with the DR6 ectodomain sequence on the assumption that DR6 and p75 binding to GFD NAPP is structurally conserved and that the binding site residues are conserved, too. Unlike the case with APLP2, however, the DR6 and p75 alignment results, as summarized in Figure 6, paint an ambiguous and difficult to interpret picture. Out of the 24 residues (96, 98–99, 103–104, 107–108, 110, 120–121, 128, 130–132, 139, 141–142, 158–159, 162–165, 167) that comprise the DR6 contribution to our model interface, only 5 (21%) are identical to the corresponding residues in p75. This is slightly less than the overall level of conservation that characterized the alignment between p75 and DR6 that was used to construct the DR6 homology model. If we include similar residues, the percentage of DR6–p75 matches increases to 37.5%. Interpretation of the results is further complicated by various nonconservative substitutions. For example, p75 substitutes an Arg for DR6 Val167 and a second Arg for DR6 Asp98. Such nonconservative substitutions could explain the reduced affinity of p75 for NAPP. In all, these results suggest that the low sequence identify either accounts for the reduced affinity of p75 for GFD NAPP, or that p75 and DR6 bind to GFD NAPP in fundamentally different ways, or that our DR6 interface predictions are inaccurate. We think the later two possibilities are unlikely given all of the evidence presented, the added complexity of assuming distinct binding geometries, and the significantly weaker binding of p75 to GFD NAPP.

To try and shed further light on all of this, we constructed a structural model of the p75–GFD NAPP interaction by structural superposition of p75 onto the DR6–GFD NAPP model (see Supporting Information). We then used

Eq. (1) to estimate the affinity of p75 for GFD NAPP. The calculated value of −7.6 kcal/mol is in excellent agreement with the experimentally derived value of −9.0 kcal/mol (see Supporting Information). This further suggests the robustness of our modeling pipeline, the basic accuracy of our DR6–GFD NAPP model and that the relatively poor interface residue conservation between p75 and DR6 probably explains the weaker affinity of p75 for NAPP.

Our DR6–GFD NAPP complex model is verified by the available theoretical data

Typically, theoretical protein–protein or protein–ligand structural models are tested against experimental mutation data.[4,8,9] Unfortunately, we were not able to locate any such data for the DR6–GFD NAPP interaction. Despite this, we were able to generate similar data using an independent computational procedure. Briefly, we used the protein–protein interaction prediction server or PPI-Pred to predict binding surfaces and thus potential interface residues for DR6 and GFD NAPP, respectively. We then compared the set of predicted interface residues, generated using PPI-Pred, with the set of interface residues derived from our model. We reasoned that good agreement between the two independently generated data sets would tend to confirm the basic accuracy of our model (Figs. 5 and 7, Tables II and III). Importantly, we first validated the procedure using the known structural interaction between the neurotrophin p75 receptor and its NGF ligand (see Supporting Information).

In the case of GFD NAPP, PPI-Pred predicated two possible binding patches (I and II); in the case of DR6, PPI-Pred predicted three possible binding patches (I, II, and III). Out of 44 PPI-Pred predicted residues for GFD NAPP, 15 agree perfectly with interface residues derived from the GFD NAPP binding interaction that characterizes our docked model. The PPI-Pred patch I and III predictions for DR6, failed to show any agreement with our docked model. The 31 PPI-Pred patch II residue predictions, however, produced 8 residue hits when compared with the DR6 residues that contribute to the interface of our docked model. Hence, many of the DR6 and GFD NAPP interface residues that characterize our docked model are also independently predicted to be interface residues. This provides still more evidence that our DR6–GFD NAPP interaction model, especially regarding the GFD NAPP contribution, is an accurate one.

The other nine ClusPro models inaccurately model the DR6–GFD NAPP interaction

ClusPro model 1 was selected for further analysis and testing because it was shown to occupy a physically plausible, deep and unique free energy minimum with respect to ClusPro complex models 2–10. In the above discussion, we have shown that model 1 is not falsified by and can be used to account for several disparate lines of evidence including binding affinity data, 22C11 antibody data, APLP2 sequence data, p75–GFD NAPP sequence and binding data, and theoretical PPI-Pred data. It is clear that models 2–10 cannot be used to account for the binding data (Fig. 3). Additional testing revealed that models 2–7 and 9 cannot be used to account for the 22C11 antibody data and that model 8 does not account for the PPI-Pred data (unpublished results). Thus, models 2–9 are inaccurate; model 1 is the best DR6–GFD NAPP model.

Random chance is a possible but unlikely explanation for our results

In all, our results clearly show the physical reasonableness and probable accuracy of our DR6–GFD NAPP interaction model. Nevertheless, it must be remembered that our model represents a hypothesis as to how DR6 and GFD NAPP interact. Thus, while there is good reason to believe that our model provides a roughly accurate picture, especially at the residue level, as to how DR6 and GFD NAPP interact to form a stable complex, we nevertheless acknowledge that it might ultimately prove to be inaccurate.[4,7] Indeed, in hindsight it can be shown that computational protein–protein models that survive a number of empirical tests can later turn out to be inaccurate. This implies that good agreement between an inaccurate protein–protein model and experiment or observation can result from random chance. Although we think it is unlikely that our results are explained by random chance, we nonetheless acknowledge the possibility and encourage caution in assessing any interpretations of or deductions from our results.

Implications of our DR6–GFD NAPP interaction model

The evidence suggests that our DR6–GFD NAPP model is of high quality and probable accuracy. Thus, it behooves us to provide an interpretation of our model and to flesh out some of its biophysical and biological implications. In what follows we assume that our model is accurate and briefly consider some of the more interesting biophysical and biological implications that are suggested by it.

Implication one

The structural-energetics of the DR6–GFD NAPP interface can be described and interpreted. Currently, there is no way to structurally and energetically rationalize DR6–GFD NAPP binding. Our model (Fig. 8) provides an opportunity to do this. GFD NAPP is 96 residues long (residues 28–123) and consists of seven beta strands and one alpha helix (66–76). The DR6 (TNFR21) ectodomain is 145 residues long (residues 67–211) and is formed by 12 beta strands. It contains 2 N-linked glycosylation sites (ASN82 and ASN 141) and nine disulfide

bonds (residues 67–80, 70–88, 91–106, 109–123, 113–131, 133–144, 150–168, 171–186, and 192–211 of CYS). The disulfide bonds provide structural stability and organize the structure into four CRDs [Fig. 8(A)]. Past work on TNF receptors indicate that the CRDs also mediate protein–protein binding interactions.[24] In the case of DR6, CRD1 includes residues 50–88, CRD2 includes residues 90–131, CRD3 spans residues 133–167, and CRD4 spans residues 170–211. Armed with a structural model of how DR6 interacts with GFD NAPP, we can now rationalize DR6–GFD NAPP binding and consider some implications in terms of these and other structural and energetic categories.

Implication two

DR6–GFD NAPP binding is primarily driven by hydrogen bonding and the hydrophobic effect. Equation (1) can be decomposed and each term analyzed to gain insight into the energetic and structural basis of binding (Table IV). The various physical descriptor values provided in Table IV are well within the ranges established by the physical descriptors derived from known protein–protein interactions. This counts as further evidence that our model is a good one. Overall, the DR6–GFD NAPP interface [Fig. 8(A)] is characterized by four salt bridges (Table V) and seven hydrogen bonds (Table VI). In terms of Eq. (1), the hydrogen bonds make a large and stabilizing contribution to binding (≈ -6.02 kcal/mol), whereas the salt bridges make a smaller contribution, especially when the cost of charge group burial is taken into consideration (≈ -1.0 kcal/mol). Thus, electrostatic complementarity and hydrogen bonding appears to play as important a role in DR6–GFD NAPP binding as it appears to play in other TNFR complexes.[22,24] According to our favored interpretation, the gap volume descriptor captures or correlates with stabilizing protein–water–protein interactions across the protein–protein interface. In the case of DR6–GFD NAPP, it appears that this favorable contribution to binding is effectively canceled by the unfavorable conformational entropy penalty of binding. Finally, some 43 hydrophobic groups are buried by DR6–GFD NAPP complex formation, contributing ≈ -3.2 kcal/mol in binding free energy. This would seem to indicate that DR6–GFD NAPP binding is strongly stabilized by the hydrophobic effect. Thus, a decomposition of Eq. (1) suggests that the DR6–GFD NAPP complex is primarily stabilized by hydrogen bonding interactions and the hydrophobic effect.

Implication three

The GFD NAPP alpha helix plays a key energetic role in DR6 recognition. Based on our model for DR6–GFD NAPP, CRD2 and CRD3 do indeed mediate DR6 binding to GFD NAPP. In particular, the CRD2-CRD3 junction appears to form a shallow depression or groove that perfectly accommodates the lone GFD NAPP alpha helix (66–76) as it is shown in Figure 8(A). In terms of atomic interactions, the GFD helix packs against disulfide bridge-stabilized DR6 beta-strand 130–132. Gln 71 of the GFD NAPP helix forms a total of three stabilizing hydrogen bonding interactions with Cys 131 and Thr 132 of the DR6 beta strand, see Figure 8(B,C) box 6. Gln 74 of the GFD NAPP alpha helix also forms an apparent hydrogen bond with Gln 139 of DR6, see Figure 8(B,C) box 2. Indeed, calculations made using Eq. (1) suggest that the GFD NAPP helix plays an important recognition role, supplying ≈ -5.0 kcal/mol in binding free energy or roughly 45% of the total binding affinity. Thus, the GFD alpha helix appears to play a key role in DR6 binding, in particular, as a recognition motif for DR6 strand 130–132. In all, a reasonable interpretation of the data is that CRD2 and CRD3 disulfide bridges 113–131 and 133–144 orient and stabilize DR6 beta strand 130–132 for thermodynamically favorable binding to GFD NAPP helix 66–76.

A network of two salt bridges and a single hydrogen bond is formed between the GFD NAPP C-terminal carboxyl group of Val 123 and the side chain of Arg 167 of DR6 as shown in Figure 8(C) box 5. This interaction is of special interest given that Val 123 occupies different positions in the unbound but high-resolution 1mwp GFD NAPP structure and the dimeric but lower resolution 3ktm NAPP structure. Thus, it appears that we got somewhat lucky in selecting the 1mwp GFD NAPP structure and that the flexibility of the GFD NAPP C-terminus may be important in DR6 recognition.

Another interesting set of atomic interactions include hydrogen bonding interactions between the DR6 side chain of Thr 163 and the GFD NAPP main chain of Ile 82, on the one hand, and the DR6 side chain of Arg 98 and the GFD NAPP main chain of Cys 62, on the other hand, see Figure 8(B,C) box 4 and box 3, respectively. The interactions are interesting because they occur on opposite sides of the GFD NAPP helix, with the former interactions positioned at the "front" of the helix and the latter positioned toward the "rear" of the helix as if they exist to correctly position and orient the GFD NAPP helix to interact with the DR6 130–132 beta strand. Indeed, the two salt bridges formed between the side chains of GFD NAPP Lys 103 and DR6 Glu 104 [Fig. 8(C) box 1], on one hand, and the previously described network of interactions between Val 123 and Arg 167, on the other, also flank either side of the GFD NAPP alpha helix and exist in a "front-to-back" orientation, thus, reinforcing the interpretation that interactions outside of the GFD NAPP alpha helix might help position it into close and stabilizing contact with the disulfide bridge-stabilized DR6 beta strand 130–132.

Implication four

DR6–GFD NAPP binding is unique and the GFD NAPP alpha helix might provide specificity to DR6 recognition. Compared to other TNFR crystallographic

binding configurations, such as p75–NGF (TNFR16-NGF) and DR5-TRAIL (TNFR10-TRAIL), the rigid-body binding orientation of the DR6–GFD NAPP interaction is unique [Fig. 8(D)]. The GFD NAPP ligand is also unique among TNFR ligands in that it is monomeric and includes alpha helical structure.[24] In addition, the GFD NAPP alpha helix appears to play an important role in providing the binding energy that drives DR6 recognition. Given that NAPP fails to bind other TNFR receptors with high affinity and given the uniqueness of its alpha helical motif, we can speculate that the GFD NAPP alpha helix also confers specificity to DR6 binding.

Implication five

Glycosylation does not appear to be involved in DR6–GFD NAPP binding. Recent work of Klima *et al.* shows that the extracellular part of the DR6 molecule is highly N- and O-glycosylated.[51] Such post-translational modifications can influence folding, transport, and function of the receptor. Glycosylation (in particular, N-linked glycosylation) could also directly regulate the affinity of the DR6 receptor for NAPP by modulating DR6–GFD NAPP interface contacts. An analysis of the available solvent-exposed ectodomain DR6 ASN residues (cross-checked at www.expasy.ch) reveals that the solvent exposed ASN residues (ASN82 and ASN141 of the DR6, see Figure 8(A) are probably too far away from and oriented away from the key DR6–GFD NAPP interface residues. Hence, our model suggests that glycosylation does not directly modulate DR6–NAPP binding. This, however, does not mean that glycosylation does not affect binding; it might affect binding through some other mechanism.

Implication six

The DR6–GFD NAPP binding reaction approximates rigid-body association and the unbound DR6 conformation is only weakly stabilized with respect to the bound conformation. The neurotrophin p75 receptor binds NGF with a free energy of binding ($\Delta G_{bind,exp}$) of ≈ -12.4 kcal/mol. Applying Eq. (1) to the 1sg1 p75–NGF coordinates yielded an estimated $\Delta G_{bind,empirical} \approx -11.8$ kcal/mol (see Supporting Information). This helps validate the use of Eq. (1) on DR6. Perhaps more importantly, given that Eq. (1) is only accurate to within ≈1.0–1.5 kcal/mol for binding reactions that approximate rigid-body association, this strongly suggests that the p75–NGF binding reaction approximates rigid-body association. This inference is further strengthened by the fact that the structure of unbound murine NGF can be superimposed to within ≈1.0 Å Ca rmsd of the common amino acids of the 1sg1 structure of bound human NGF.[22] We were also able to use Eq. (1) to accurately estimate the binding affinity of the DR6–GFD NAPP binding reaction. Moreover, as described above, the bound and unbound conformations of GFD NAPP are nearly identical. Thus, the DR6–GFD NAPP reaction probably approximates rigid-body association. Therefore, the unbound or native state conformation of DR6 (and p75) is probably stable with respect to the bound conformation by ≈1.0–1.5 kcal/mol.

Implication seven

A structurally modest binding associated acquisition of beta structure in DR6 residues 130–132 may provide a conformational switch for cellular apoptosis. p75 and DR6 binding probably approximate rigid-body association and their unbound conformations are probably ≈1.0–1.5 kcal/mol stable with respect to their bound conformations. For rigid-body association, our published and unpublished work suggests that binding associated conformational changes with respect to unbound conformations are typically <1.5 Å Ca rmsd. Thus, the binding associated p75 and DR6 structural transitions probably involve modest conformational rearrangements on the order of 1.5 Ca Å rmsd.[19] This inference appears to be consistent with the modest p75–NGF binding associated gain in secondary structure suggested by a spectroscopic analysis of p75–NGF binding.[52] Given the evidence, we can reasonably speculate that DR6 residues 130–132 are the primary residues that undergo a modest binding associated reorganization from a relatively unstructured state to a beta-structured bound state. All of this suggests that NAPP binding to DR6 mediates cellular apoptosis through a structurally subtle acquisition of beta structure in DR6 residues 130–132.

Implication eight

The unbound (pro-life) DR6 conformation is only weakly stabilized with respect to the DR6 bound (pro-death) conformation and this suggests spontaneous apoptosis for a nontrivial number of DR6-sensitive cells. Because ligand binding to p75 and DR6 leads to apoptosis through caspase mediation, we can refer to the unbound conformations as pro-life conformations and the bound conformations as pro-death conformations. As discussed previously, it can be argued that rigid-body association for p75 and DR6 suggests that their unbound conformations (pro-life conformations) are only weakly stabilized with respect to their bound (pro-death conformations) conformations (≈1.0−1.5 kcal/mol) and are structurally similar, at least in terms of Ca rmsd calculations. Thus, in the absence of pro-death signaling (no GFD NAPP) and for purely "intrinsic" biophysical reasons, we would expect roughly 8.0–16.0% of DR6 (and p75) receptors to spontaneously adopt subtly different pro-death conformations and, in the absence of some other mechanism, to spontaneously engage the cells apoptotic machinery, culminating in cell death (see Supporting Information). Thus, in the absence of some other mechanism, a nontrivial fraction of DR6 (and p75) sensitive cells would be expected to fall victim to spontaneous

apoptosis, through a subtle change in ectodomain conformation and in the absence of ligand binding. It is worth noting that this is consistent with what is known about the roughly 15% of neutrophil cells that undergo spontaneous apoptosis through caspase mediation but in the absence of ligand-death receptor binding.[53–55]

Implication nine

Our DR6–GFD NAPP model should prove useful in suggesting future experiments, in rationalizing other results and in structure b-based AD drug design. The model provides a structural basis for future experimental testing and possible refinement. For example, interface mutagenesis experiments could be run to test and possibly refine the model. The model also provides a basis for designing experiments to test other DR6- and GFD NAPP-related hypotheses and to possibly rationalize data that we have failed to consider. Perhaps most importantly, the model can be used in structure-based design studies aimed at identifying drug-like compounds to modulate DR6–GFD NAPP binding and possibly treat AD.

LIMITATIONS OF THIS STUDY

One concern about this study has to do with the multimethod nature of the modeling pipeline we used. Although this is a legitimate concern, we think our modeling pipeline is reasonable, especially in light of previous work and the validation study we did on p75–NGF (see Supporting Information). Moreover, each step in the modeling pipeline has been extensively tested and reported on in the scientific literature. It is also worth recalling that numerous multimethod and fruitful studies have been reported in the literature. As a recent example, the ClusPro developers have favorably reported on their experience in CAPRI rounds 13–19, a round that included the use of a computationally demanding post-ClusPro modeling workflow and homology model docking.[56] Finally, the success of our proposed DR6–GFD NAPP model is hard to reconcile with a fundamentally flawed modeling pipeline and final modeling result.

A second concern about this study has to do with the problem of error accumulation and propagation, especially as it pertains to the MM-GB/SA calculations that we used to select the best DR6–GFD NAPP model. The concern is that large error bars would prevent us from rationally preferring one docked model over others. First, we think this concern is mitigated by noting that the MM-GB/SA calculations were used to eliminate obvious non-binders and not as a quantitative estimate of the binding affinity. Nevertheless, a recent analysis suggests MM-GB/SA error ranges can easily approach $\pm$5.0 kcal/mol, even for relatively small ligands.[57] Thus, it must be admitted that such uncertainty could interfere with our ability to definitively reject models 2, 3, and 9 on the basis of our $\Delta G_{\text{bind,MM-GB/SA}} < 0$ kcal/mol criterion [Fig. 3(C)]. Importantly, the conclusions of this study are unaffected by such error considerations, as final model selection was performed using Eq. (1), with a known error of $\approx$1.0–1.5 kcal/mol. In the future, greater care will have to be exercised in the use of absolute MM-GB/SA values. In fact, error considerations seem to favor the use of relative MM-GB/SA values, as they probably involve error subtraction.

An important assumption is our equating EC50 values with k_d values. This identification rests on several assumptions, including reversible binding, single site binding, that the measured ELISA signal is proportional to receptor occupancy and, finally, that there is negligible ligand combination in the assay. It is further assumed that ligand labeling and receptor immobilization is not problematic. Nonetheless, it is reasonable to assume a simple binding model and to equate the reported EC50 values with k_d values. At least four reasons can be given for this. First, Nikolaev *et al.* used a straightforward DR6–NAPP ELISA binding assay, and the calculated hyperbolic binding curves are consistent with a simple binding model. Second, the assumed k_d value for the DR6–GFD NAPP interaction is reasonable given the binding free energies of other TNFR interactions. Third, we used Eq. (1) to accurately calculate the isothermal titration calorimetry determined binding affinity of the p75–NGF interaction (see Supporting Information). Finally, we were also able to apply Eq. (1) to a model of the p75–GFD NAPP interaction and successfully predict the relative EC50 of the reaction with respect to the DR6–GFD NAPP reaction (see Supporting Information). Thus, it is reasonable to assume a simple binding model and to equate EC50 values with k_d values.

A final limitation is worth calling attention to. Ideally, we would have been able to compare the hypothesized DR6 contribution to binding with experimental data that implicated specific DR6 residues in a manner analogous to the 22C11 GFD NAPP antibody data. In the absence of such a comparison, the hypothesized GFD NAPP residue level contribution to binding stands on firmer experimental ground than does the hypothesized DR6 contribution.

CONCLUSIONS

Nikolaev et al. have proposed a biochemical model of neuronal development that may have implications for AD. Key to their model is a novel interaction between the DR6 ectodomain and an N-terminal fragment of APP (NAPP), with particular emphasis on the GFD NAPP. The elucidation of the structural basis of the DR6–GFD NAPP interaction could pave the way towards an improved understanding of neuronal development, an improved understanding of AD pathophysiology and innovative pharmacological therapies for AD. As such, we used a pure computational work-flow that integrated homology modeling, docking and free energy scoring to

model the interaction between a refined homology model of DR6 and a crystal structure of GFD NAPP. The use of high quality binding competent structures, a proven rigid-body docking methodology, a well-tested refinement procedure, and an exhaustively tested empirical free energy scoring methodology, all combined to produce a final high quality model of probable a priori structural accuracy. We then tested and verified, a posteriori, the model against a variety of biophysical and theoretical data sets. Finally, assuming the model to be accurate, we provided a structural-energetic interpretation of DR6–GFD binding and derived some biophysical and biological predictions from the model. In conclusion, the proposed DR6–GFD NAPP model, especially regarding the residue-level contribution of GFD NAPP, is a high quality model of probable structural accuracy that has not been falsified by the available data. Rather, the evidence suggests that our model can be used to rationalize quite a bit of data, and that it can be reasonably interpreted on structural, biophysical, and biological grounds. Finally, the model can be used to suggest the real possibility of GFD NAPP or ligand induced apoptosis and non-GFD NAPP or spontaneous apoptosis through subtle DR6 ectodomain conformational rearrangements.

ACKNOWLEDGMENTS

The authors would like to thank Dr. Anatoly Nikolaev, Genentech Inc., for the valuable discussions and suggestions on the topic of AD. J.A. supervised the project, predicted the binding affinities (scoring function), prepared the tables and some figures, edited the Supporting Information and wrote the paper. S.Y.P. proposed the basic research idea, performed most of the molecular modeling procedures (homology modeling, docking, minimization), prepared a majority of the figures, wrote the Supporting Information, and proof read the manuscript.

REFERENCES

1. Nikolaev A, McLaughlin T, O'Leary DD, Tessier-Lavigne M. APP binds DR6 to trigger axon pruning and neuron death via distinct caspases. Nature 2009;457:981–989.
2. Berchanski A, Lapidot A. Computer-based design of novel HIV-1 entry inhibitors: neomycin conjugated to arginine peptides at two specific sites. J Mol Model 2009;15:281–294.
3. Berchanski A, Lapidot A. Prediction of HIV-1 entry inhibitors neomycin-arginine conjugates interaction with the CD4-gp120 binding site by molecular modeling and multistep docking procedure. Biochim Biophys Acta 2007;1768:2107–2119.
4. Chapman BS, Kuntz ID. Modeled structure of the 75-kDa neurotrophin receptor. Protein Sci 1995;4:1696–707.
5. Litjens SH, Wilhelmsen K, de Pereda JM, Perrakis A, Sonnenberg A. Modeling and experimental validation of the binary complex of the plectin actin-binding domain and the first pair of fibronectin type III (FNIII) domains of the beta4 integrin. J Biol Chem 2005;280:22270–22277.
6. Nomme J, Renodon-Cornière A, Asanomi Y, Sakaguchi K, Stasiak AZ, Stasiak A, Norden B, Tran V, Takahashi M. Design of potent inhibitors of human RAD51 recombinase based on BRC motifs of BRCA2 protein: modeling and experimental validation of a chimera peptide. J Med Chem 2010;53:5782–5791.
7. Shamovsky IL, Ross GM, Riopelle RJ, Weaver DF. The interaction of neurotrophins with the p75NTR common neurotrophin receptor: a comprehensive molecular modeling study. Protein Sci 1999;8:2223–2233.
8. Walters DE, Hellekant G. Interactions of the sweet protein brazzein with the sweet taste receptor. J Agric Food Chem 2006;54:10129–10133.
9. Yi H, Qiu S, Cao Z, Wu Y, Li W. Molecular basis of inhibitory peptide maurotoxin recognizing Kv1.2 channel explored by ZDOCK and molecular dynamic simulations. Proteins 2008;70:844–854.
10. Martin OA, Villegas ME, Aguilar CF. Three-dimensional studies of pathogenic peptides from the c-terminal of Trypanosoma cruzi ribosomal P proteins and their interaction with a monoclonal antibody structural model. PMC Biophys 2009;2:4.
11. Lensink MF, Mendez R, Wodak SJ. Docking and scoring protein complexes: CAPRI, 3rd Edition. Proteins 2007;69:704–718.
12. Lensink MF, Wodak SJ. Docking and scoring protein interactions: CAPRI 2009. Proteins 2010;78:3073–3084.
13. Sircar A, Gray JJ. SnugDock: paratope structural optimization during antibody-antigen docking compensates for errors in antibody homology models. PLoS Comput Biol 2010;6:e1000644.
14. Vajda S, Kozakov D. Convergence and combination of methods in protein-protein docking. Curr Opin Struct Biol 2009;19:164–170.
15. Halperin I, Ma B, Wolfson H, Nussinov R. Principles of docking: an overview of search algorithms and a guide to scoring functions. Proteins 2002;47:409–443.
16. Moitessier N, Englebienne P, Lee D, Lawandi J, Corbeil CR. Towards the development of universal, fast and highly accurate docking/scoring methods: a long way to go. Br J Pharmacol 2008;153 (Suppl 1):S7–S26.
17. Audie J. Continued development of an empirical function for predicting and rationalizing protein-protein binding affinities. Biophys Chem 2009;143:139–144.
18. Audie J. Development and validation of an empirical free energy function for calculating protein-protein binding free energy surfaces. Biophys Chem 2009;139:84–91.
19. Audie J, Scarlata S. A novel empirical free energy function that explains and predicts protein-protein binding affinities. Biophys Chem 2007;129:198–211.
20. Rossjohn J, Cappai R, Feil SC, Henry A, McKinstry WJ, Galatis D, Hesse L, Multhaup G, Beyreuther K, Masters CL, Parker MW. Crystal structure of the N-terminal, growth factor-like domain of Alzheimer amyloid precursor protein. Nat Struct Biol 1999;6:327–331.
21. Berman HM, Westbrook J, Feng Z, Gilliland G, Bhat TN, Weissig H, Shindyalov IN, Bourne PE. The Protein Data Bank. Nucleic Acids Res 2000;28:235–242.
22. He XL, Garcia KC. Structure of nerve growth factor complexed with the shared neurotrophin receptor p75. Science 2004;304:870–875.
23. Matrone C, Ciotti MT, Mercanti D, Marolda R, Calissano P. NGF and BDNF signaling control amyloidogenic route and Abeta production in hippocampal neurons. Proc Natl Acad Sci USA 2008;105:13139–13144.
24. Zhang G. Tumor necrosis factor family ligand-receptor binding. Curr Opin Struct Biol 2004;14:154–160.
25. Dahms SO, Hoefgen S, Roeser D, Schlott B, Gührs KH, Than ME. Structure and biochemical analysis of the heparin-induced E1 dimer of the amyloid precursor protein. Proc Natl Acad Sci USA 2010;107:5381–5386.
26. Humphrey W, Dalke A, Schulten K. VMD: visual molecular dynamics. J Mol Graph 1996;14:33–38, 27–28.
27. Guex N, Peitsch MC. SWISS-MODEL and the Swiss-PdbViewer: an environment for comparative protein modeling. Electrophoresis 1997;18:2714–2723.
28. Roy A, Kucukural A, Zhang Y. I-TASSER: a unified platform for automated protein structure and function prediction. Nat Protoc 2010;5:725–738.
29. Zhang Y. I-TASSER: fully automated protein structure prediction in CASP8. Proteins 2009;77 (Suppl 9):100–113.

30. Zhang Y. I-TASSER server for protein 3D structure prediction. BMC Bioinformatics 2008;9:40.
31. Zhang Y. Template-based modeling and free modeling by I-TASSER in CASP7. Proteins 2007;69 (Suppl 8):108–117.
32. Benkert P, Kunzli M, Schwede T. QMEAN server for protein model quality estimation. Nucleic Acids Res 2009;37(Web Server issue): W510–W514.
33. Benkert P, Tosatto SC, Schomburg D. QMEAN: a comprehensive scoring function for model quality assessment. Proteins 2008;71: 261–277.
34. Wiederstein M, Sippl MJ. ProSA-web: interactive web service for the recognition of errors in three-dimensional structures of proteins. Nucleic Acids Res 2007;35(Web Server issue):W407–W410.
35. Zhou H, Zhou Y. Distance-scaled, finite ideal-gas reference state improves structure-derived potentials of mean force for structure selection and stability prediction. Protein Sci 2002;11:2714–2726.
36. Alberghina L, Colangelo AM. The modular systems biology approach to investigate the control of apoptosis in Alzheimer's disease neurodegeneration. BMC Neurosci 2006;7 (Suppl 1):S2.
37. Comeau SR, Gatchell DW, Vajda S, Camacho CJ. ClusPro: a fully automated algorithm for protein-protein docking. Nucleic Acids Res 2004;32 (Web Server issue): W96–W99.
38. Comeau SR, Gatchell DW, Vajda S, Camacho CJ. ClusPro: an automated docking and discrimination method for the prediction of protein complexes. Bioinformatics 2004;20:45–50.
39. Bradford JR, Westhead DR. Improved prediction of protein-protein binding sites using a support vector machines approach. Bioinformatics 2005;21:1487–1494.
40. Comeau SR, Kozakov D, Brenke R, Shen Y, Beglov D, Vajda S. ClusPro: performance in CAPRI rounds 6–11 and the new server. Proteins 2007;69:781–785.
41. Comeau SR, Vajda S, Camacho CJ. Performance of the first protein docking server ClusPro in CAPRI rounds 3–5. Proteins 2005;60: 239–244.
42. Zacharias M. Protein-protein docking with a reduced protein model accounting for side-chain flexibility. Protein Sci 2003;12: 1271–1282.
43. Gong Y, Cao P, Yu HJ, Jiang T. Crystal structure of the neurotrophin-3 and p75NTR symmetrical complex. Nature 2008;454:789–793.
44. Chothia C, Lesk AM. The relation between the divergence of sequence and structure in proteins. EMBO J 1986;5:823–826.
45. Ring CS, Sun E, McKerrow JH, Lee GK, Rosenthal PJ, Kuntz ID, Cohen FE. Structure-based inhibitor design by using protein models for the development of antiparasitic agents. Proc Natl Acad Sci USA 1993;90:3583–3587.
46. Chopra G, Summa CM, Levitt M. Solvent dramatically affects protein structure refinement. Proc Natl Acad Sci USA 2008;105: 20239–20244.
47. Summa CM, Levitt M. Near-native structure refinement using in vacuo energy minimization. Proc Natl Acad Sci USA 2007;104: 3177–3182.
48. Summa CM, Levitt M, Degrado WF. An atomic environment potential for use in protein structure prediction. J Mol Biol 2005;352:986–1001.
49. Duan Y, Reddy BV, Kaznessis YN. Physicochemical and residue conservation calculations to improve the ranking of protein-protein docking solutions. Protein Sci 2005;14:316–328.
50. Li L, Chen R, Weng Z. RDOCK: refinement of rigid-body protein docking predictions. Proteins 2003;53:693–707.
51. Klima M, et al. Functional analysis of the posttranslational modifications of the death receptor 6. Biochim Biophys Acta 2009;1793: 1579–1587.
52. Timm DE, Vissavajjhala P, Ross AH, Neet KE. Spectroscopic and chemical studies of the interaction between nerve growth factor (NGF) and the extracellular domain of the low affinity NGF receptor. Protein Sci 1992;1:1023–1031.
53. Lee D, Long SA, Adams JL, Chan G, Vaidya KS, Francis TA, Kikly K, Winkler JD, Sung CM, Debouck C, Richardson S, Levy MA, DeWolf WE Jr, Keller PM, Tomaszek T, Head MS, Ryan MD, Haltiwanger RC, Liang PH, Janson CA, McDevitt PJ, Johanson K, Concha NO, Chan W, Abdel-Meguid SS, Badger AM, Lark MW, Nadeau DP, Suva LJ, Gowen M, Nuttall ME. Potent and selective nonpeptide inhibitors of caspases 3 and 7 inhibit apoptosis and maintain cell functionality. J Biol Chem 2000;275:16007–16014.
54. Scheel-Toellner D, Wang K, Assi LK, Webb PR, Craddock RM, Salmon M, Lord JM. Clustering of death receptors in lipid rafts initiates neutrophil spontaneous apoptosis. Biochem Soc Trans 2004;32(Pt 5):679–681.
55. Goepel F, Weinmann P, Schymeinsky J, Walzog B. Identification of caspase-10 in human neutrophils and its role in spontaneous apoptosis. J Leukoc Biol 2004;75:836–843.
56. Kozakov D, Hall DR, Beglov D, Brenke R, Comeau SR, Shen Y, Li K, Zheng J, Vakili P, Paschalidis ICh, Vajda S. Achieving reliability and high accuracy in automated protein docking: ClusPro, PIPER, SDU, and stability analysis in CAPRI rounds 13–19. Proteins 2010;78:3124–3130.
57. Merz KM. Limits of free energy computation for protein-ligand interactions. J Chem Theory Comput 2010;6:1018–1027.